RSC Medicinal Chemistry

ROYAL SOCIETY OF CHEMISTRY

RESEARCH ARTICLE

View Article Online
View Journal | View Issue

Open Access Article. Published on 28 October 2024. Downloaded on 12/5/2025 5:05:15 PM.
This article is licensed under a Creative Commons Attribution-NonCommercial 3.0 Unported Licence.

Check for updates

Cite this: *RSC Med. Chem.*, 2025, **16**, 747

meso-Substituted AB_3-type phenothiazinyl porphyrins and their indium and zinc complexes photosensitising properties, cytotoxicity and phototoxicity on ovarian cancer cells†

Brém Balázs,[a] Bianca Stoean (Vasile),[a] Éva Molnár,[a] Eva Fischer-Fodor,[b] Ovidiu Bălăcescu,[b] Raluca Borlan,[c] Monica Focsan,[cd] Adriana Grozav,[e] Patriciu Achimaş-Cadariu,[bf] Emese Gál*[a] and Luiza Gaina*[a]

Received 3rd August 2024,
Accepted 27th October 2024

DOI: 10.1039/d4md00601a

rsc.li/medchem

New *meso*-substituted AB_3-type phenothiazinyl porphyrins and ferrocenylvinyl phenothiazinyl porphyrin were synthesised by Suzuki–Miyaura and Mizoroki–Heck cross-coupling reactions, respectively. The free porphyrins were further used in the synthesis of new indium(III) or zinc(II) porphyrin complexes. All porphyrins exhibit red fluorescence emission in solution, a property that remains unimpaired following internalisation in ovarian A2780 cancer cells, as evidenced by fluorescence microscopy images. The In(III) phenothiazinyl porphyrin complexes show a higher quantum yield of fluorescence emission (**2a** Φ_F = 30%, **4a** Φ_F = 29%, **5a** Φ_F = 28%) compared to the free base porphyrin precursors, or Zn(II) complex **4b** (Φ_F = 10%). The potential of novel phenothiazinyl porphyrins to act as photosensitisers was evaluated using two distinct approaches. The first was through the measurement of the singlet oxygen quantum yield $\Phi_\Delta(^1O_2)$, while the second employed *in vitro* measurements of metabolic activity, oxidative stress, nuclear factor-erythroid 2 related factor 2 (Nrf-2) activation and tumour necrosis factor-alpha (TNF-α) under both dark and light irradiation conditions. As reflected by the IC_{50} values, the most potent cytotoxicity of the phenothiazinyl porphyrins against the A2780 cells was observed for In(III) ferrocenylvinyl phenothiazinyl porphyrin **4a** (36.38 μM), the remaining compounds are less cytotoxic. The reduction in metabolic activity was observed in A2780 ovarian tumour cells treated with **4a** and **6a** and exposed to light compared to treatment in the absence of light. The oxidative stress, TNF-α and Nrf-2 transcription factor were particularly notable when A2780 cells were treated with **4a** and subsequently photoirradiated, the oxidative stress was linked to the highest value of $\Phi_\Delta(^1O_2)$ recorded for **4a** (60%).

1. Introduction

The emerging techniques of photodynamic diagnosis (PDD) and photodynamic therapy (PDT)[1] have the potential to enhance early detection, treatment and surveillance of various malignant conditions. These methodologies entail the incorporation of photosensitizer compounds within tumour cells, which are then selectively activated through a variety of light-emitting sources. Extensive investigations have been undertaken to assess their efficacy across diverse cancer types, including gynaecological malignancies.

A number of porphyrin-based photosensitizers have been approved by the Food and Drug Administration (FDA) for clinical use.[2] These include porfimer sodium, temoporfin and padeliporfin, the latter of which is a new and promising structure that contains the transition metal palladium for the purpose of achieving enhanced biological outcomes.

Ovarian cancer is one of the most prevalent malignant neoplasms in women, with a high mortality rate due to its

[a] *Research Center on Fundamental and Applied Heterochemistry, Faculty of Chemistry and Chemical Engineering, Babeş-Bolyai University, 11 Arany Janos str, RO-400028 Cluj-Napoca, Romania. E-mail: emese.gal@ubbcluj.ro, ioana.gaina@ubbcluj.ro; Tel: +40 264 593833*
[b] *Institute of Oncology "Prof. Dr. Ion Chiricuta", RO-400015 Cluj-Napoca, Romania*
[c] *Nanobiophotonics and Laser Microspectroscopy Centre, Interdisciplinary Research Institute on Bio-Nano-Sciences, Babes-Bolyai University, 42 Treboniu Laurian Street, 400271, Cluj-Napoca, Romania*
[d] *Biomolecular Physics Department, Faculty of Physics, Babes-Bolyai University, 1 M. Kogalniceanu Street, 400084, Cluj-Napoca, Romania*
[e] *Faculty of Pharmacy, "Iuliu Hatieganu" University of Medicine and Pharmacy, Victor Babes 41, RO-400012 Cluj-Napoca, Romania*
[f] *Department of Oncological Surgery and Gynecological Oncology, "Iuliu Hatieganu" University of Medicine and Pharmacy, RO-400012 Cluj-Napoca, Romania*

† Electronic supplementary information (ESI) available. See DOI: https://doi.org/10.1039/d4md00601a

Open Access Article. Published on 28 October 2024. Downloaded on 12/5/2025 5:05:15 PM.
This article is licensed under a Creative Commons Attribution-NonCommercial 3.0 Unported Licence.

tendency to be diagnosed in advanced stages and frequently demonstrate chemoresistance to various chemotherapeutic agents. Consequently, there have been numerous endeavours to utilise photosensitizers for the preoperative identification of tumours, the detection of metastatic lesions during surgical procedures and the enhancement of antitumour chemotherapy.[1] It has been extensively demonstrated that oxidative stress plays a pivotal role in the induction of programmed cell death and drug resistance in ovarian cancer cells.[3] It has been demonstrated that porphyrin-based photosensitizers[4] elevate the level of reactive oxygen species (ROS) under specific wavelength light irradiation. Consequently, targeting ROS levels in ovarian cancer may prove an effective strategy for counteracting drug resistance.[5]

The production of ROS at the mitochondrial level is regulated by the nuclear erythroid-related factor-2 (Nrf2), a transcription factor responsible for protecting cells against oxidative stress. Elevated ROS levels activate Nrf2; consequently, the overexpression of Nrf2 is responsible for the development of chemoresistance, which inactivates the drug-mediated oxidative stress that could otherwise result in cancer cell death.[6]

Tetraphenyl-porphyrin photosensitizers can be readily incorporated into living cells and target subcellular compartments, particularly the mitochondria.[7] When exposed to specific light irradiation, including infrared light sources, these photosensitizers act as ROS inducers. The porphyrin derivatives have been demonstrated to exhibit photoactivity against microorganisms,[8] tumour cells for *in vitro* experiments,[9–13] or *in vivo*[14] in animal models. Most of them are theragnostic agents with specific colours, characteristic emissions and biodistribution, so they can be used not only as photodynamic activators but also as bioimaging agents, and some of them are suitable for magnetic resonance probes.[15] Grafting metals onto these structures, such as indium,[12] zinc[16] and metallocene,[11,17] can improve their anti-tumour potential in PDT.

The use of indium porphyrins in cancer or antimicrobial photodynamic therapy (PDT) is becoming increasingly attractive due to their ability to generate singlet oxygen and reactive oxygen species (ROS).[18] The complexation of a porphyrin analogues with a heavy metal, such as indium, palladium or gallium, has a significant impact on FRET (Förster resonance energy transfer), which is associated with singlet oxygen generation and *in vivo* PDT efficacy. Of the metals tested, the In(III) complex demonstrated the most promising results with regard to cancer imaging and PDT efficacy, when compared with gallium and palladium.[19] The enhanced singlet oxygen generation was observed in indium tetraphenyl porphyrin nanostructures,[20] in $Ag/CuFe_2O_4$ nanoparticles containing cationic indium porphyrin[21] and in the gold nanoparticles containing indium thienylporphyrins.[22]

Phenothiazine derivatives are known to be effective photosensitizers, as they are involved in the generation of singlet oxygen.[23,24] Cationic dyes with a phenothiazinium chromophore system are among the most extensively studied photosensitizers, methylene blue (MB) is a particularly prominent representative in this group. The MB and its analogues have been demonstrated to function as photosensitizers in photodynamic therapy,[25–28] as well as in industrial applications.[29] An additional crucial aspect is the capacity of phenothiazine derivatives to permeate tumour cells. This was demonstrated by the FLIM technique in phenothiazine vinyl pyridinium dyes, which were *in vitro* internalized in B16-F10 melanoma cells[30] and methylene blue analogues, which were also found to be internalized in A2780 and OVCAR-3 human ovarian cancer cells.[31] Experiments conducted *in vitro* using *meso*-phenothiazinyl-porphyrin derivatives have demonstrated that the phenothiazinyl-porphyrin derivatives are capable of inducing a phototoxic effect on epidermoid carcinoma A431 cells in PDT experiments under blue and red-light irradiation.[32]

The capacity of *meso*-substituted phenothiazinyl-porphyrin derivatives to be internalised into ovarian human cells[13] and generate singlet oxygen represents an asset in the development of novel potential conjugated drugs for photodynamic therapy. The objective of this research was to design and synthesise novel AB_3 *meso*-substituted phenothiazinyl-porphyrins and their indium and zinc complexes. This was done with the aim of developing photosensitizers for singlet oxygen generation and investigating dark toxicity and phototoxicity on ovarian cancer cells. In this context, we evaluated the capacity of a series of novel porphyrins and metalloporphyrins to generate singlet oxygen in solution and to exert photodynamic potential *in vitro* on A2780 ovarian cancer cells, with a particular focus on their capacity to be incorporated into ovarian tumour cells for the purpose of reducing mitochondrial metabolism, triggering ROS and modulating Nrf-2, NF-κB and TNF-α in both dark and photoactivated status.

2. Result and discussion

2.1 Chemistry

A series of *meso*-substituted AB_3-type phenothiazinyl-porphyrins **2**, **4**, **5** and their metal complexes **2a**, **4a**,**b**, **5a** were prepared to investigate the photosensitising properties, cytotoxicity and phototoxicity on A2780 ovarian cancer cells. The new *meso*-substituted AB_3-type phenothiazinyl-porphyrins **2** and **4** were obtained by cross-coupling reactions from AB_3-type *meso*-substituted halogeno-porphyrin derivatives, the free base porphyrins **2** and **4** were subsequently employed in the complexation reaction.

The synthesis of phenothiazinyl-porphyrin **2** was achieved through a Suzuki–Miyaura cross-coupling reaction, utilising AB_3-type bromophenyl-porphyrins and phenothiazinyl-boronic acid esters **1**. The subsequent complexation reaction of free base porphyrin **2** was conducted with indium tetrachloride, resulting in the generation of indium(III) phenothiazinyl-porphyrin **2a**, Scheme 1.

The free base porphyrin **4** was obtained by a Mizoroki–Heck cross-coupling reaction, in which vinylferrocene

 This journal is © The Royal Society of Chemistry 2025

Open Access Article. Published on 28 October 2024. Downloaded on 12/5/2025 5:05:15 PM.
This article is licensed under a Creative Commons Attribution-NonCommercial 3.0 Unported Licence.

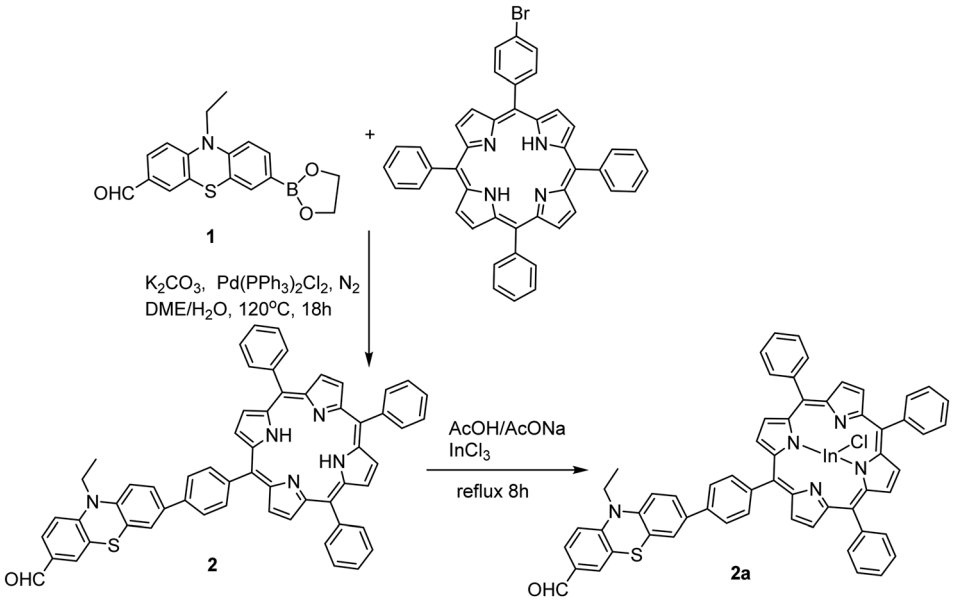

Scheme 1 Synthesis of *meso*-substituted phenothiazinyl-porphyrin **2** by Suzuki–Miyaura cross-coupling reaction, and it's In(III) complex **2a**.

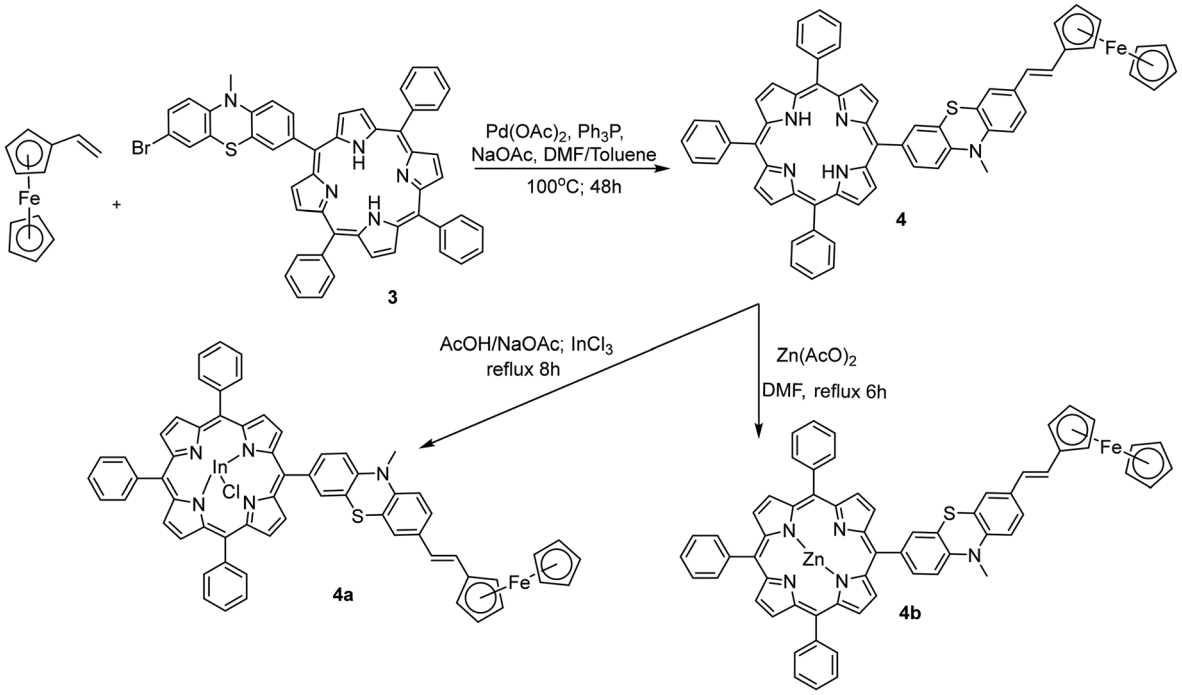

Scheme 2 Synthesis of *meso*-substituted ferrocenylvinyl-phenothiazinyl-porphyrin **4** by Mizoroki–Heck cross-coupling reaction and it's In(III) and Zn(II) complexes **4a**, **4b**.

replaced the bromine atom on bromophenothiazinyl-porphyrin **3** in the presence of a base and a palladium catalyst. The free base of ferrocenylvinyl-phenothiazinyl-porphyrin **4** was subsequently employed in the synthesis of the indium(III) phenothiazinyl-porphyrin **4a** and zinc phenothiazinyl-porphyrin **4b**, as depicted in Scheme 2.

The *meso*-substituted AB_3-type phenothiazinyl-bromophenylporphyrin **5** and tetraphenylporphyrin TPP **6** were complexed with indium tetrachloride to obtain the corresponding indium(III) porphyrins derivatives **5a** and **6a**, respectively, as shown in Scheme 3.

The structure of the newly synthesised porphyrins **2**, **4** and new metalloporphyrins **2a**, **4a**,**b**, **5a** was confirmed based on nuclear magnetic spectroscopy (NMR) and high-resolution mass spectrometry (HRMS), (ESI† Fig. S1–S21). In the ^{1}H-NMR spectra, the specific signal of inner core porphyrin

Open Access Article. Published on 28 October 2024. Downloaded on 12/5/2025 5:05:15 PM.
This article is licensed under a Creative Commons Attribution-NonCommercial 3.0 Unported Licence.

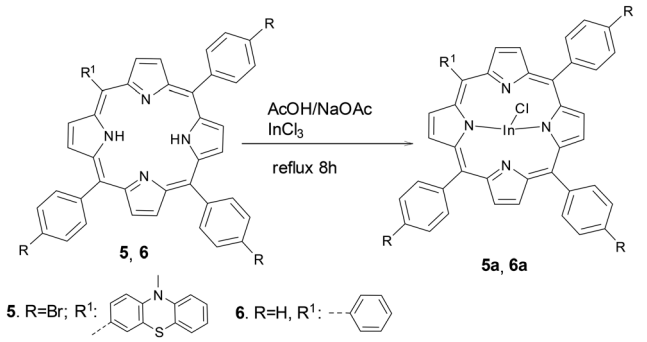

Scheme 3 Synthesis of *meso*-substituted porphyrins by complexation of free porphyrin base with $InCl_3$.

protons exhibited a singlet at −2.74 ppm in porphyrins **2** and **4** and −2.80 ppm in porphyrin **5**. The absence of the singlet of inner core porphyrin protons in the ^{1}H-NMR spectra for metalloporphyrins **2a**, **4a**,**b**, **5a** is consistent with the results of the HRMS spectra, indicating that the complexation reaction was occurring.

The In(III) tetraphenyl porphyrin chloride **6a** and its precursor tetraphenyl porphyrin **6** (TPP) were employed to examine the impact of the indium(III) ion's presence within the central porphyrin core. The peripheral substituents in the *meso*-position (phenothiazine and ferrocene) were investigated regarding their impact on the efficacy of the porphyrins as photosensitizers for singlet oxygen generation and cyto- and phototoxicity on the A2780 ovarian carcinoma cell line.

2.2 Optical properties

The photophysical properties of newly synthesised porphyrins and metalloporphyrins were investigated by UV-vis and fluorescence spectroscopic methods. The UV-vis absorption spectra exhibited the characteristic Soret band for free base porphyrins and metalloporphyrins, which was observed at approximately 420–425 nm and characterised by a high molar extinction coefficient (3.7×10^5–2.52×10^5 M^{-1} cm^{-1}).

Furthermore, for the free-base porphyrin derivatives four low-intensity *Q* bands were observed in the visible spectral region between 515–649 nm, as shown in Fig. 1a and Table 1. However, only two such *Q* bands were observed for the metalloporphyrin derivatives at 560 and 601 nm, which is indicative of a successful complexation reaction, as illustrated in Fig. 1b and Table 1.

It was demonstrated that the investigated *meso*-substituted porphyrins, encompassing both the free bases and their metal complexes, exhibited an emission maximum between 649–656 nm when excited at the Soret wavelength. Enhanced fluorescence emission was observed for the In(III) porphyrin complexes **2a** (Φ_F = 30%), **4a** (Φ_F = 29%), **5a** (Φ_F = 28%), **6a** (Φ_F = 22%) compared to the corresponding porphyrin free base (**2**, Φ_F = 1%, **4** and **5** Φ_F = 3%, **6** Φ_F = 11%). A comparative analysis of fluorescence emission between metal complexes of ferrocenyl phenothiazinyl porphyrin **4** with indium **4a** and zinc **4b** reveals that the In(III) porphyrin **4a**, Φ_F = 29%, exhibits enhanced fluorescence quantum yield in comparison to the Zn(II) porphyrin **4b**, Φ_F = 10%, as illustrated in Fig. 2 and Table 1.

In addition, the solvatochromism of porphyrins **5** and **5a** in DMSO, a more polar aprotic solvent than DCM, was investigated by UV-vis absorption and fluorescence emission spectroscopy. It was observed that the absorption and emission wavelengths showed a similar trend, with the absorption and emission wavelengths having similar values in both solvents, (ESI† Fig. S22).

2.3 Singlet oxygen generation

To quantify the photosensitising efficiency of the porphyrins and metalloporphyrin, the quantum yield of singlet oxygen

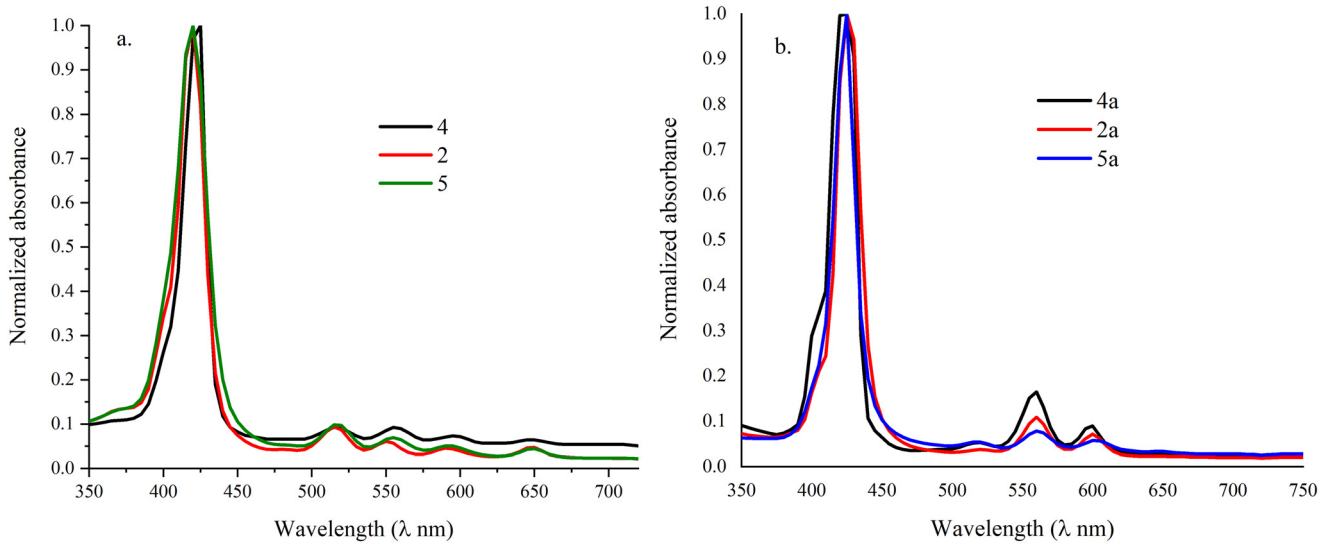

Fig. 1 The UV-vis absorption spectra of: (a) free base porphyrins **2**, **4**, **5** and (b) In(III) porphyrin derivatives **2a**, **4a**, **5a**, recorded in DCM (~10^{-4} M).

Open Access Article. Published on 28 October 2024. Downloaded on 12/5/2025 5:05:15 PM.
This article is licensed under a Creative Commons Attribution-NonCommercial 3.0 Unported Licence.

Table 1 The absorption and emission data of free base porphyrin and their metal complexes recorded in dichloromethane DCM at 10^{-5} M

Cpd.	λ_{abs} [nm] Soret[a] (ε mol^{-1} cm^{-1})	Q_4	Q_3	Q_2	Q_1	λ_{em} [nm]	Stokes shift cm^{-1}	Φ_F[b]	$\Phi_\Delta(^1O_2)$ relative singlet oxygen quantum yield[c]
2	**420** (371 000)	516	550	590	649	653	8495	0.01	0.17
2a	**425** (311 000)	561	601			654	8262	0.30	0.07
4	**423** (252 000)	517	557	595	649	652	8303	0.03	0.12
4a	**424** (236 000)	562	596			654	8294	0.29	0.60
4b	**420** (262 000)	550	590			649	8401	0.10	0.29
5	**420** (329 000)	517	555	593	646	656	8565	0.03	0.08
5a	**423** (274 000)	560	601			655	8350	0.28	0.04
6a	**425** (434 000)	560	598			651	8168	0.22	0.74

[a] λ_{ex} wavelength employed for excitation in fluorescence experiments and Stokes shift calculation. [b] Quantum yields calculated using TPP compound **6** as a standard in dichloromethane (CH_2Cl_2, abbreviation DCM), Φ_F = 0.11. [c] Calculated using **6** (TPP) as a standard $\Phi_\Delta(^1O_2)$ = 0.52.[33]

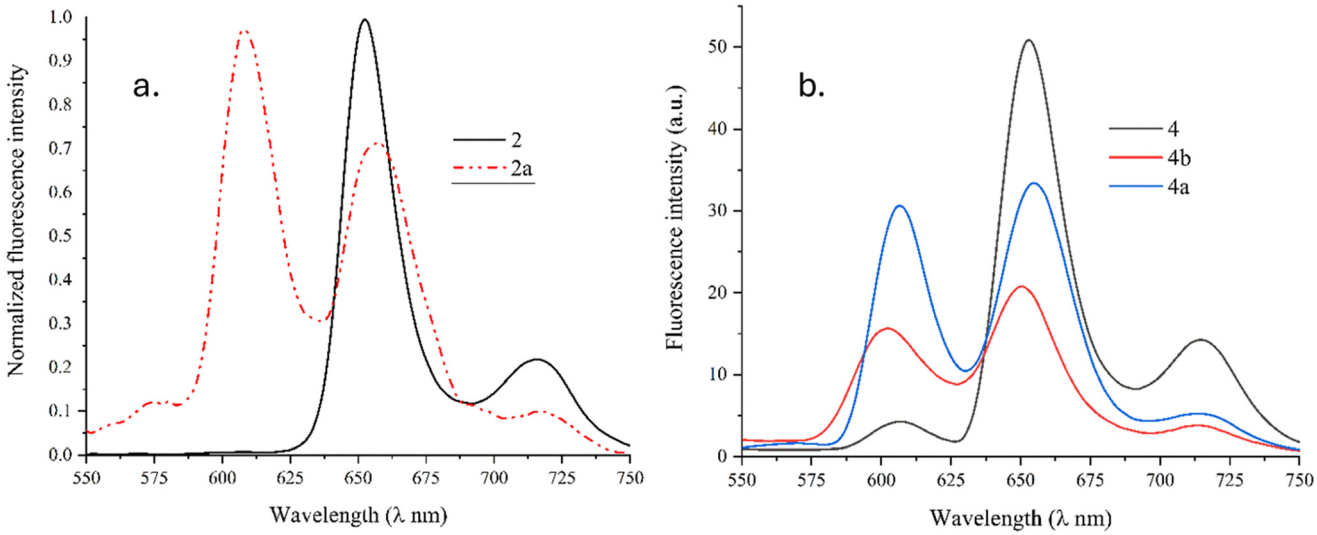

Fig. 2 The fluorescence emission spectra of new porphyrins: (a) **2**, **2a** and (b) **4**, **4a**,**b**, recorded in dichloromethane.

generation $\Phi_\Delta(^1O_2)$ was evaluated using an indirect detection protocol based on the chemical reaction of $^1O_2$ with 1,3-diphenylisobenzofuran (DPBF). This method was employed to estimate the amount of $^1O_2$ generated in the presence of photosensitizers **2**, **2a**, **4**, **4a**,**b**, **5**, **5a**, **6a** during LED irradiation at 505 nm. The selection of 505 nm as the excitation wavelength was based on the rationale that it falls within the resonance absorption range of all the photosensitizers under investigation. By minimizing variations in absorption efficiency across different compounds, the use of 505 nm excitation enables a more accurate assessment of the intrinsic ability of each photosensitizer to generate $^1O_2$. Tetraphenyl porphyrin (TPP) **6** was used as a reference, to analyse the influence of peripheral substituents and inner core metalation concerning the ability to generate $^1O_2$ under light irradiation. The absorption spectra of DPBF in the presence of porphyrin derivatives show a significant decrease in the DPBF absorbance maximum at 417 nm over a total irradiation period of 150 seconds at a wavelength of 505 nm, as shown in Fig. 3. The reduction in the DPBF absorbance maximum is due to the reaction of DPBF with $^1O_2$ generated by the energy transfer from the excited triple state of *meso*-substituted porphyrins to oxygen molecules.

The relative $^1O_2$ quantum yield, $\Phi_\Delta(^1O_2)$, was analysed for free base porphyrins **2**, **4**, **5** and their indium (**2a**, **4a**, **5a**, **6a**) and zinc (**4b**) complexes (Fig. 3, Table 1). The highest value was found for In(III) tetraphenyl porphyrin **6a** (74%), followed by In(III) ferrocenyl-phenothiazinyl-porphyrin **4a** (60%), while the remaining compounds exhibited values below the standard TPP **6**. The In(III) complexes of *meso*-substituted AB_3-type phenothiazinyl-porphyrins **2a** ($\Phi_\Delta{}^1O_2$ = 7%) and **5a** ($\Phi_\Delta{}^1O_2$ = 4%) display a lower $\Phi_\Delta(^1O_2)$ values than their corresponding free base porphyrins **2** ($\Phi_\Delta{}^1O_2$ = 17%), and **5** ($\Phi_\Delta{}^1O_2$ = 8%), in these cases, the presence of indium(III) ion does not have a positive effect on the $^1O_2$ generation. Nevertheless, a higher $\Phi_\Delta(^1O_2)$ is observed for the In(III) complex **4a** (60%) compared to Zn(II) complex **4b** (29%), both of which are complexes of the free base ferrocenyl-phenothiazinyl-porphyrin **4** (12%), in this case the increase

Open Access Article. Published on 28 October 2024. Downloaded on 12/5/2025 5:05:15 PM.
This article is licensed under a Creative Commons Attribution-NonCommercial 3.0 Unported Licence.

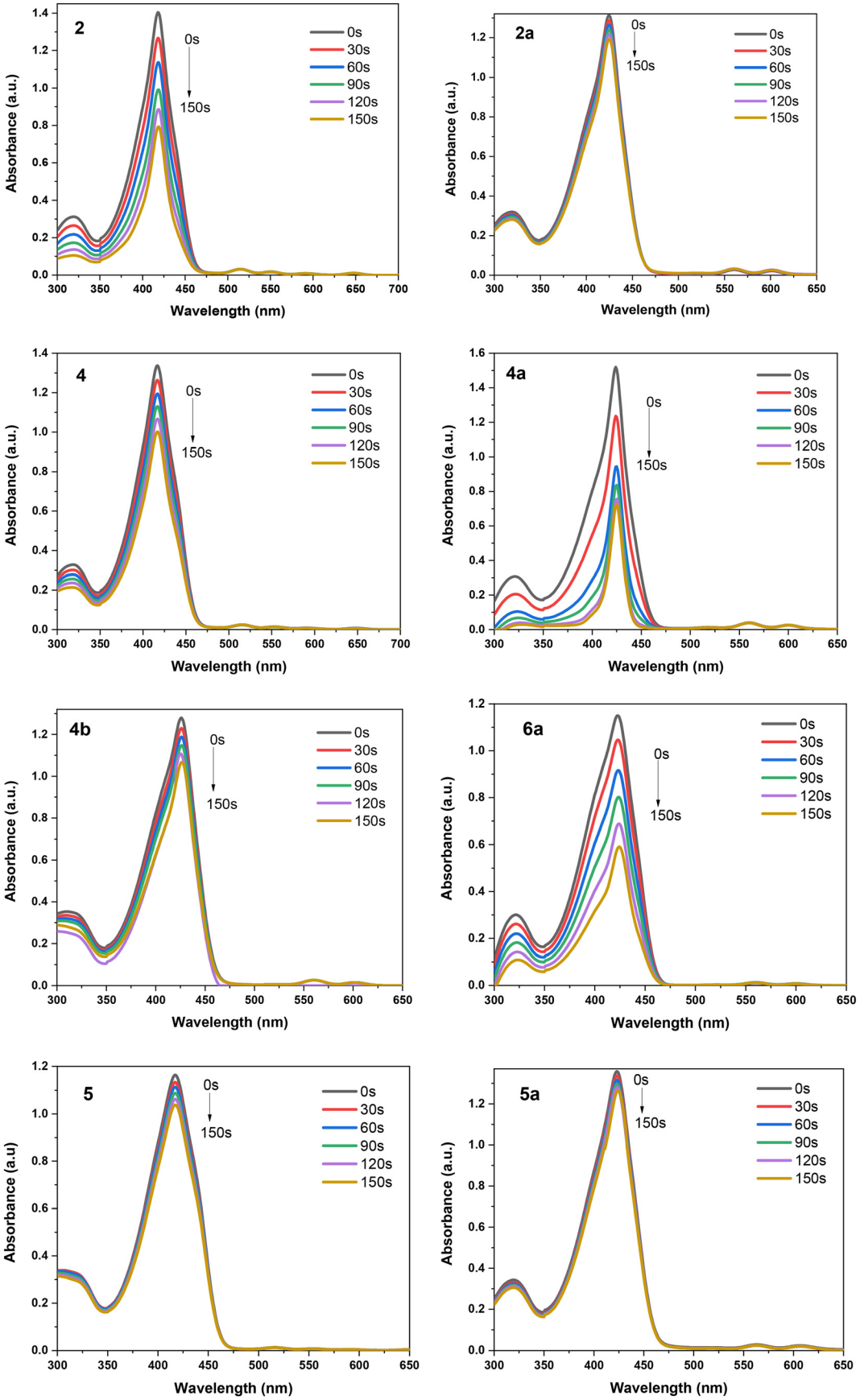

Fig. 3 Absorption spectra of DPBF at different time points (0, 30, 60, 90, 120, and 150 seconds) in the presence of porphyrin derivatives **2**, **2a**, **4**, **4a**,**b**, **6a**, **5**, **5a**, in DMSO, while exposed to a LED light emitted by a 505 nm.

Open Access Article. Published on 28 October 2024. Downloaded on 12/5/2025 5:05:15 PM.
This article is licensed under a Creative Commons Attribution-NonCommercial 3.0 Unported Licence.

in $\Phi_{\Delta}(^1O_2)$ can be attributed to the contribution of the indium ion.

Similar values of the singlet oxygen quantum yield have been reported for other In(III) *meso*-substituted porphyrins such as tetrakis(4-(methylthio)phenyl)porphyrin ($\Phi_{\Delta}(^1O_2)$ 54%), or porphyrins containing a heterocyclic moiety like tetra(thiophen-2-yl)porphyrin ($\Phi_{\Delta}(^1O_2)$ 73%),[22] but the fluorescence quantum yield was considerably lower compared to In(III) complexes of *meso*-substituted phenothiazinyl porphyrins.

2.4 Cell growth inhibition

The capacity of the *meso*-substituted porphyrins to inhibit the growth of A2780 ovarian cancer cells after a 24 hour exposure was evaluated using the MTT colorimetric test. The values obtained from the porphyrin derivative (Table 2) were compared with those of the precursor TPP porphyrin and the standard antitumor chemotherapeutic drug carboplatin.

The cytotoxicity of the compounds was reflected by their individual IC_{50} values. The lowest IC_{50} value was observed for **4a** (36.38 μM), which exhibited the most potent toxicity against the A2780 cells, similarly, **6a** (45.91 μM) demonstrated a high degree of cytotoxicity, both compounds having indium as central atom.

Compounds **4a**, **4b** and **4**, which occupy positions 1, 3 and 5 in this hierarchy, are all compounds with a ferrocenyl Cp_2-Fe moiety, where **4a** contains In(III), **4b** contains Zn(II) and **4** it's the free base. The highest cytotoxicity observed for **4a** compared to its analogues **4** and **4b** is probably mainly due to the indium ion.

The standard porphyrin toxicity TPP **6** "threshold" (144.05 μM) is below **4a**, **6a**, **4b**, while **2**, **2a**, **5**, and **5a** are less cytotoxic, all above 250 μM, this includes **2a** (287.84 μM) and **5a** (459.56 μM) which contain the central metal indium(III). In the dark, the presence of indium(III) ion in the porphyrin structure does not guarantee an anti-cancer activity, **2a** and **5a** being representative examples of this group. These results show that not only the central ion but also the peripheral substituents from the *meso* position of the porphyrin unit influence the CI_{50} value.

Table 2 The cytotoxicity of the porphyrins and the reference materials, expressed as half maximal inhibitory concentration (IC_{50}, micromolar), derived from the sigmoidal dose–response curves as presented in the ESI† (Fig. S23); the standard error (SE) of log IC_{50} was calculated in the 95% confidence interval

Compound	IC_{50} (μM)	Log IC_{50}	SE log IC_{50}
2	**255.30**	2.407	0.091
2a	**287.84**	2.459	0.103
4	**176.6**	2.247	0.058
4b	**114.06**	2.057	0.040
4a	**36.38**	1.561	0.060
5	**321.26**	2.507	0.104
5a	**459.56**	2.662	0.276
TPP **6**	**144.05**	2.158	0.048
6a	**45.91**	1.662	0.026
Carboplatin	**79.53**	1.901	0.045

2.5 Cellular uptake of porphyrin and metalloporphyrin derivatives

A2780 cells were treated with a sublethal concentration of 20 μM of compounds **2**, **2a**, **4**, **4a**,**b**, **5**, **5a**, **6a** and TPP **6** (used as reference) in cell culture medium for 24 hours and 72 hours, respectively. All compounds were able to internalise into A2780 ovarian tumour cells. The internalisation of the indium-containing complexes (**4a**, **2a**, **5a** and **6a**) is shown in Fig. 4I and II. The cellular uptake of **4**, **4b**, **2**, **5**, and TPP **6** is shown in ESI† Fig. S24 and S25.

The differences in the density of the cell populations are a consequence of the different survival rates after treatment with 20 μM solution of **2a**, **4a**, **6a** and **5a**. Since **6a** and **4a** exhibit higher cytotoxicity (low IC_{50} values), fewer cells remained attached to the plate after 24 hours of treatment compared to cell populations treated with **2a** or **5a**. The red fluorescent porphyrins are evenly distributed in the cell populations despite their density on the plates. This intense fluorescence in the cytoplasm and relatively constant distribution of the compounds is present not only in A2780 cells treated with indium-functionalised **6a**, **4a**, **2a** and **5a**, (Fig. 4II) but also with the other four compounds (ESI† Fig. S25).

2.6 Alteration of mitochondrial function by porphyrin treatment and photoirradiation

The cells metabolic activity is influenced by a range of treatments and light sources, and this parameter was evaluated using the resazurin-based Alamar Blue method, which measures the mitochondrial reducing activity of A2780 cells. The ovarian tumour cells were either treated with one of the porphyrins at sub-lethal concentrations (5; 25 and 50 μM) under normal conditions, avoiding exposure to white light and any other light source, and designated as the "dark" group. Alternatively, they were treated and irradiated with a LED light source at λ = 505 nm (after 24 hours of incubation with porphyrins at sub-lethal concentrations), and designated as the "PDT" group, Fig. 5.

The metabolic rate of the treated cells was calculated against the untreated control cell population. In the case of photoirradiated samples, the reference was the metabolic rate of the untreated, photoirradiated cells (Fig. 5). The variations in metabolic rate relative to compound concentration can be quantified using linear regression curves (dotted lines on all cartridges of Fig. 5). For each linear regression, the following parameters were generated by the statistics software: the hillslope, the F of unequal variance and the p values of the reduction significance, data presented in ESI† Table S1. The curves representing the metabolic rate variations exhibit a descending tendency when the concentration of porphyrin increases (negative hillslope, ESI† Table S1). Following light irradiation of the A2780 cells treated with **4a** and **6a**, a notable decline in metabolic activity was observed. Conversely, the presence of **2**, **2a**, **4**, **4b**, and **5** resulted in a more modest reduction in metabolic activity (ESI† Fig. S30). The porphyrins **4a** and **6a**, which contain

Open Access Article. Published on 28 October 2024. Downloaded on 12/5/2025 5:05:15 PM.
This article is licensed under a Creative Commons Attribution-NonCommercial 3.0 Unported Licence.

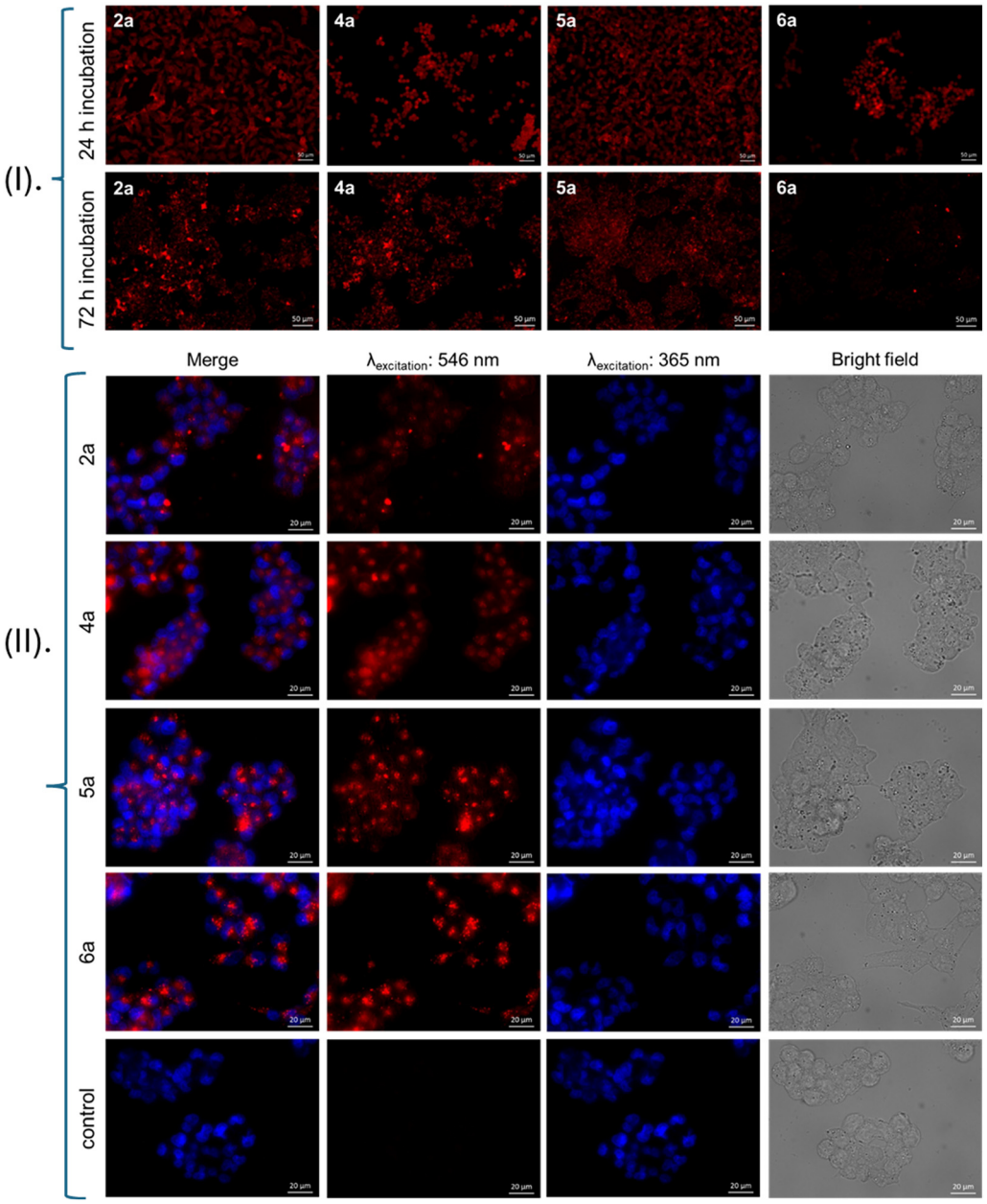

Fig. 4 (I) Fluorescence microscopy images of A2780 cells treated with porphyrin derivatives **2a**, **4a**, **5a**, and **6a** at a final concentration of 20 μM under standard cell culture conditions (37 °C, 5% CO_2), incubated for 24 (top) and 72 hours (bottom). (II) Fluorescence microscopy images of A2780 cells after 72 hours treatment with 20 μM derivatives **2a**, **4a**, **5a**, **6a**, and an untreated control, in comparison with their corresponding bright field images.

indium as the central metal, exhibit an improvement in their A2780 toxicity profile when subjected to photoirradiation (PDT) in comparison to their behaviour in the absence of light. The presence of the ferrocene moiety in the studied porphyrins **4**, **4a**,**b**, acts as an enhancer of the toxicity in the dark, and will improve the antitumor activity after light exposure only when indium is present in the molecule.

In the case of **5a**, the presence of the indium ion in the porphyrin core does not induce a significant cytotoxic effect when compared with all the other compounds under investigation. However, an enhancement in its toxicity profile was observed when the compound was subjected to photoirradiation (PDT), in comparison to its behaviour in the absence of light.

After the evaluation at 24 hours, the metabolic activity of the cells was tracked for 72 hours, using four distinct concentrations, in triplicate replicates $n = 9$ (Fig. 6 and S30†). The treatment was completed with the concentrations of 5; 15; 25 and 50 μM for each compound, in triplicates, and the cells reduction capacity-based metabolic activity was measured at 24, 48 and 72 hours, respectively. The In(III) complexes **4a**, **6a**, **5a** and **2a** were depicted in Fig. 6, while the

 This journal is © The Royal Society of Chemistry 2025

Open Access Article. Published on 28 October 2024. Downloaded on 12/5/2025 5:05:15 PM.
This article is licensed under a Creative Commons Attribution-NonCommercial 3.0 Unported Licence.

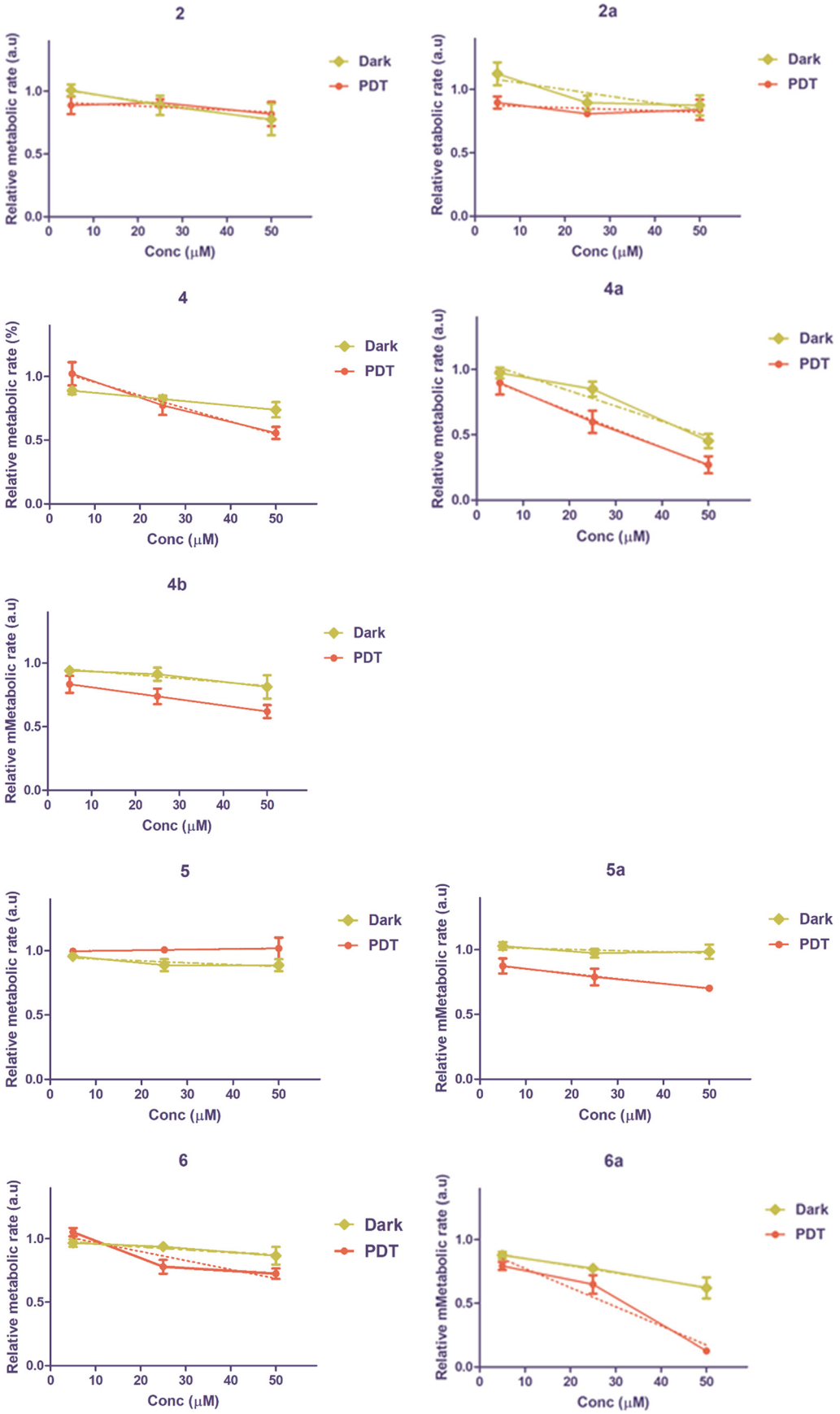

Fig. 5 Variations of metabolic activity in A2780 cells treated with sublethal concentration of **2**, **2a**, **4**, **4a**,**b**, **5**, **5a**, **6a** and TPP **6** in dark, and photoirradiated abbreviated PDT (LED irradiation λ = 505 nm, time 150 s), respectively.

Open Access Article. Published on 28 October 2024. Downloaded on 12/5/2025 5:05:15 PM.
This article is licensed under a Creative Commons Attribution-NonCommercial 3.0 Unported Licence.

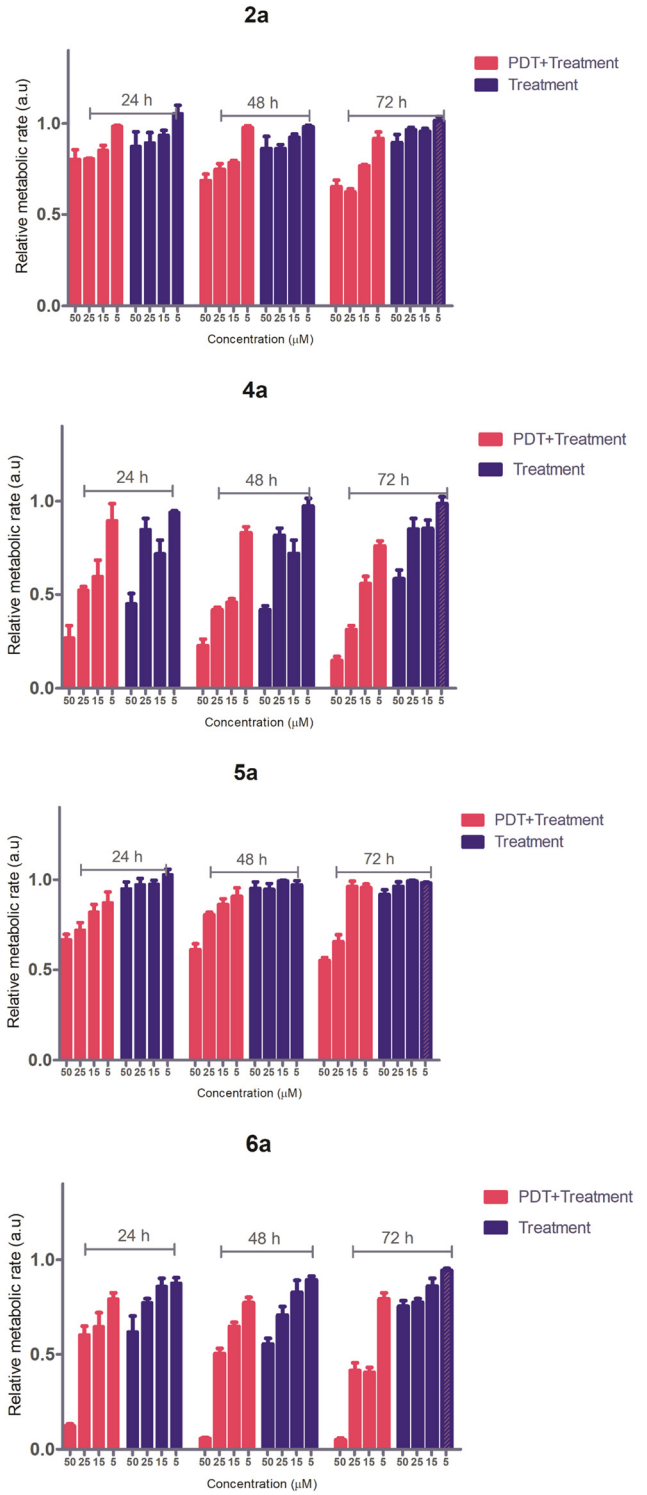

Fig. 6 The metabolic rate evolution of treated A2780 cells, within 72 hours interval, in the presence or absence of photoirradiation (PDT). Compounds **2a**, **4a**, **5a** and **6a** were assessed at the concentrations of 5; 15; 25 and 50 μM, and the measurements were made at 24, 48 and 72 hours.

other phenothiazinyl-porphyrins were depicted in ESI† Fig. S30. The activity of the compounds is dose-dependent, but not time-dependent; in the absence of photoirradiation, most of the compounds exhibit their best inhibitory effect after 24 hours of monitoring. The compounds **2a** and **5a** exhibit very slight effect after 48 or 72 hours at these sublethal concentrations. Compound **4a** maintain somewhat of its inhibitory capacity especially when subjected to 50 or 25 μM concentration, while **6a** activity became moderate at 72 hours, even at 50 μM concentration. The compounds which exhibited poor inhibitory activity at 24 hours, after 48 or 72 hours were almost inactive due to the rapid proliferation rate of A2780 cell line.

Instead, when treatment was followed by photoirradiation, a certain time dependency was observed, with cells being more affected by photoirradiation after a longer incubation period (Fig. 8). The metabolic activity of A2780 cells subjected to **4a** and **6a** remain diminished after 48 hours, and this tendency continues after 72 hours. Also, the 50 and 25 μM concentrations of **5a** and **2a** continues to exert inhibition after 48 and even 72 hours.

2.7 The oxidative stress in treated ovarian cancer cells

Tetraphenyl porphyrin (TPP) and its metal complexes have been demonstrated to function as photosensitizers in human tumour cells. This is based on their capacity to generate reactive oxygen species (ROS), such as singlet oxygen.[8,34,35] Building on the capacity of *meso*-substituted porphyrins and their metal complexes to generate ROS, further investigation was conducted into the production of ROS induced by *meso*-substituted phenothiazinyl porphyrins free bases and their metal complexes in the dark or under light irradiation.

The production of reactive oxygen species (ROS) generated with and without photoirradiation was monitored in A2780 cells after 24 hours of treatment with a sublethal concentration of 20 μM porphyrin derivatives **2**, **2a**, **4**, **4a**,**b**, **5**,

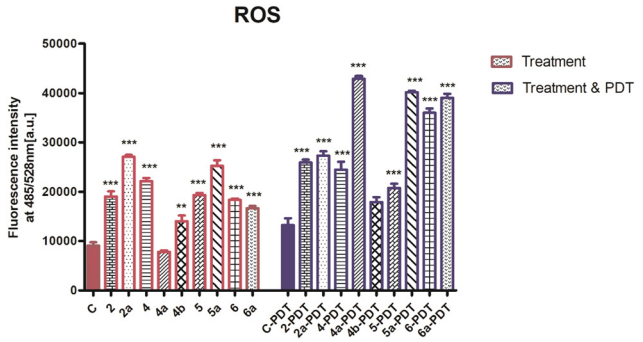

Fig. 7 The reactive oxygen species (ROS) level in A2780 cells treated with 20 μM **2**, **2a**, **4**, **4a**,**b**, **5**, **5a**, **6a** or TPP **6** in dark conditions *versus* light irradiation (abbreviated PDT), as indicated by the fluorescence intensity of the samples. The following abbreviations were used: **2**, **2a**, **4**, **4a**,**b**, **5**, **5a**, **6**, **6a** correspond to the A2780 cells treated with the compounds, TPP **6** is the reference tetraphenylporphyrin, C the untreated control, C-PDT the untreated and photoirradiated control while **2-PDT**, **2a-PDT**, **4-PDT**, **4a-PDT**, **4b-PDT**, **5-PDT**, **5a-PDT**, **6-PDT**, **6a-PDT** is the code for the samples treated and photoirradiated. The starred columns represent statistically significant increases in ROS production.

 This journal is © The Royal Society of Chemistry 2025

Open Access Article. Published on 28 October 2024. Downloaded on 12/5/2025 5:05:15 PM.
This article is licensed under a Creative Commons Attribution-NonCommercial 3.0 Unported Licence.

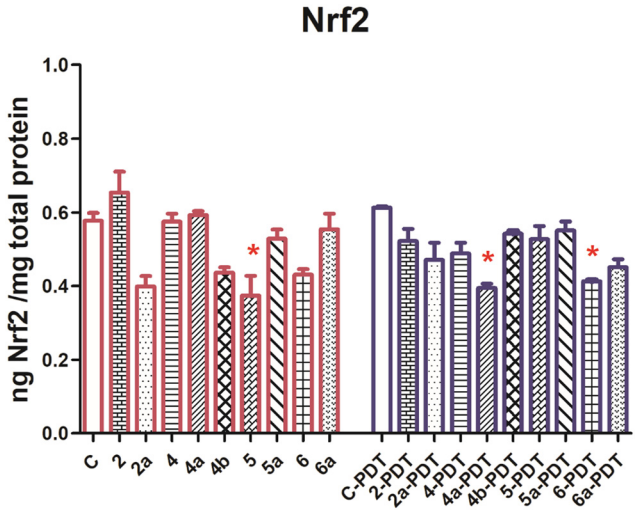

Fig. 8 Quantitative evaluation of intracellular Nrf2 modulation following the A2780 cell populations treatment with the compounds **2**, **2a**, **4**, **4a**, **4b**, **5**, **5a**, **6** and **6a** in absence (abbreviated as **2** to **6a**) or presence of photoirradiation (abbreviated as **2-PDT** to **6a-PDT**). Significant reduction of Nrf2 expression were highlighted with red starring: **5** *versus* the reference untreated cells, and respectively **4a-PDT** and **6-PDT** *versus* untreated irradiated cells.

5a, **6a** and TPP **6**. This was conducted using a standard fluorescence test (CM-H2DCFDA), as described in the Methods section 4.9. The measurements were normalised according to the viability of the cell populations in each individual sample.

The oxidative stress generated in A2780 ovarian cancer cell cultures treated with porphyrins **2**, **2a**, **4**, **4b**, **5**, **5a**, **6**, **6a** induces significant amounts of reactive oxygen species as quantified by fluorescence (Fig. 7, One-way ANOVA test, *** extremely significant, $p < 0.001$, ** very significant, $p < 0.01$), with the exception of **4a**. Compared to the reference TPP **6**, compounds **2a**, **5a** and **4** showed higher levels of ROS, while in **4b** and **4a** treated samples the ROS levels were significantly lower (One-way ANOVA test, Bonferroni post-test, in the 95% confidence interval). Following photoirradiation, ROS level exhibited an increase in all samples, including those that had not been treated, when compared with samples that had been treated in the dark. Apart from **4b-PDT**, all treated and irradiated samples exhibited a significantly higher ROS production than the control. TPP **6-PDT** demonstrated a particularly notable increase, given its designation as a photo-activator. The oxidative stress response of compounds **6a-PDT**, **4a-PDT**, and **5a-PDT** to the A2780 ovarian cancer cells was found to be comparable to that of tetraphenyl porphyrin **6-PDT**.

2.8 Modulation of nuclear factor erythroid 2-related factor 2 (Nrf2) and nuclear factor kappa light chain enhancer of activated B cells (NF-κB)

An elevated Nrf-2 can induce ovarian tumour cells to become resistant to metal-based drugs. This is achieved by modulating the membrane transporters responsible for the cellular uptake of platinum drugs and other metal drugs.

It was previously demonstrated that Nrf-2 is highly expressed in A2780 cells. In addition to its role in ROS-induced cell signalling, Nrf-2 has been implicated in the platinum-based drug resistance of ovarian cancer, due to the activation of ABCF2 (ref. 36) and ABCG2 (ref. 5) drug extrusion membrane proteins of the ATP-binding cassette (ABC) transporter family, both of which are present in A2780 ovarian cancer cells.[36] Furthermore, Nrf-2 has been demonstrated to impede the solute carrier SLC40A1, an iron transporter that has been implicated in the incorporation of metal drugs in A2780 and other ovarian tumour cells.[37]

The A2780 ovarian cancer cell line has a constitutive expression of Nfr2 (ref. 6) and the treatment with the porphyrins, including the reference TPP were able to influence the intracellular level of this transcription factor (Fig. 8).

The basal Nrf2 value of 0.577 ng mg^{-1} total protein in untreated A2780 cells was moderately augmented by **4a** and **2**, while the rest of the compounds diminished Nrf2. In the absence of irradiation, only the decrease observed following treatment with porphyrin **5** was statistically significant, according to one-way analysis of variance and Bonferroni post-test, $p < 0.05$.

Compared to the dark-treated cells, the general trend of Nrf2 levels was a decrease when the cells were treated and then photoirradiated, as shown in Fig. 8 and S26.† The untreated reference value was 0.613 ng mg^{-1} protein, which represents a statistically insignificant change in Nrf2 expression in A2780 cells.

After photoirradiation, **4a-PDT** and TPP **6-PDT** were able to significantly reduce the Nrf2 levels associated with the untreated photoirradiated cells, and the difference between the downregulation of Nrf2 by **4a-PDT** and **4a** in dark conditions was statistically significant (One-way analysis of variance, Bonferroni post-test, $p < 0.05$; Fig. 8 and S26†). In all other sets of dark *vs.* irradiated samples, this relationship was not demonstrated.

Instead, the transcription factor NF-κB p65 subunit was not significantly modulated by any of the compounds, and the photoirradiation does not changed this tendency (data presented in ESI,† Fig. S29). At the concentration of 20 μM and 24 hours exposure, NF-κB p65 values are slowly higher in irradiated cells, in compare with the cells subjected only to treatment with compounds **2** to **6a**, but they do not converge with Nrf-2, ROS or other parameters linked to cell death induction in A2780 cells, therefore in A2780 cells no NF-κB mediated cell death mechanisms will occur, while treated with these low concentrations, therefore it is other ROS-linked pathway.

2.9 The influence on the tumour necrosis factor-alpha (TNF-α)

Tumour necrosis factor alpha is an important proinflammatory cytokine, and it was proven that its secretion increases *in vitro* but also in the patients serum,

Open Access Article. Published on 28 October 2024. Downloaded on 12/5/2025 5:05:15 PM.
This article is licensed under a Creative Commons Attribution-NonCommercial 3.0 Unported Licence.

when ovarian cancer patients were treated with certain chemotherapy schemes, including carboplatin and docetaxel.[38] The TNF-α level secreted by the untreated A2780 cells is usually low, the values can increase time-dependently, or following the treatment with various cytostatic drugs.[39]

The sublethal concentration of 20 μM phenothiazinyl-porphyrins was able to induce changes in TNF-α secretion in the tumour cells; the treatment with **4a**, **4b**, **6a** and the ref. 6 caused significant increase of TNF-α (Fig. 9). When the treatment was applied alongside with light irradiation, all compounds induced a significant increase *versus* the irradiated untreated reference samples, except **5-PDT**, where a decrease was noticed. The evolution of TNF-α concentration in the photoirradiated cells is well correlated ($p < 0.05$) with the Nrf-2 and ROS level in the cells subjected to the same treatment and photoirradiation (ESI† Fig. S27).

Consequently, by targeting ROS signalling and Nrf-2 transcription factor, and by the induction of proinflammatory signals *via* TNF-α the effectiveness of the drugs, particularly those based on metals, can be enhanced. This has been achieved by irradiating the A2780 cells treated with porphyrins **4a**, **6a** and, to some extent, **2a**, all three compounds contain an indium(III) ion in their molecules, with **4a** additionally containing an iron(II) ion in the ferrocenyl Cp_2Fe unit.

The oxidative stress and Nrf-2 activation were particularly notable when A2780 cells were treated with **4a** and subsequently photoirradiated. The observed synergy can be attributed to the presence of the ferrocenyl group in conjunction with indium in this molecule. The experimental evidence indicates that the presence of Cp_2Fe alone in the studied porphyrin structures does not guarantee antitumor photodynamic activation. Among ferrocenyl-functionalized porphyrins, the second-best activity following photodynamic therapy belongs to **4b**, a molecule bearing both Cp_2Fe and a zinc(II) ion. However, it still falls below TPP in oxygen singlet generation and Nrf-2 triggering and is only weakly activated following irradiation.

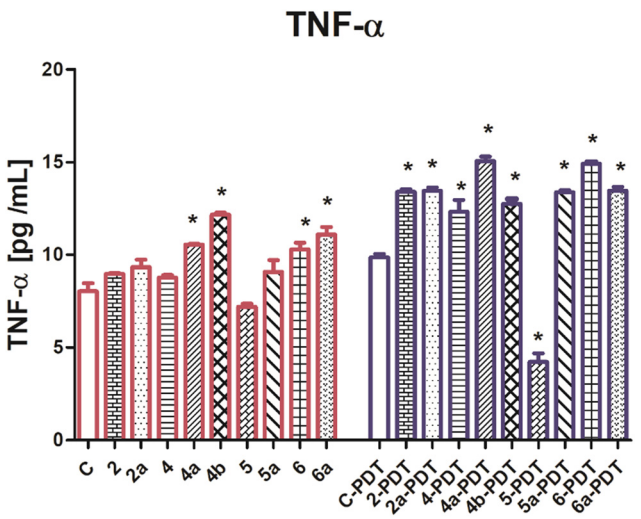

Fig. 9 The level of TNF-α secreted by A2780 ovarian tumour cells, following the treatment with the compounds **2**, **2a**, **4**, **4a**, **4b**, **5**, **5a**, **6** and **6a** in absence (abbreviated as **2** to **6a**) or presence of photoirradiation (abbreviated as **2-PDT** to **6a-PDT**). The starred columns indicate significant increase or decrease of extracellular TNF-α, induced by compounds and irradiation, within 24 hours.

A statistical analysis of the biologic features (ESI† Fig. S27a.-i.) revealed several correlations between the data. The cytotoxicity of the compounds correlates well with the decrease in the metabolic rate of tumour cells, both in dark conditions and photoirradiation (ESI† Fig. S7a and d). It also correlates with the amount of reactive oxygen species (ROS) generated in dark conditions (ESI† Fig. S27c and e) and with the relative singlet oxygen yield of the compounds (ESI† Fig. S27h). An intriguing correlation can be observed between IC_{50} values and the tendency of Nrf2 to increase after photoirradiation (ESI† Fig. S27b) and in the absence of photoirradiation. This implies that compounds with lower IC_{50} values, such as **6a**, **4b** or **4a**, will exhibit less Nrf2 after irradiation. Consequently, they may be able to circumvent the protective antiapoptotic effect of Nrf2. The porphyrin derivatives **2**, **2a**, **2**, **4a**,**b**, **5**, **5a**, **6a** demonstrated a capacity to produce singlet oxygen species outside the cells, as measured using 1,3-diphenylisobenzofuran (DPBF) substrate. This capacity exhibited a tendency to increase in the same manner inside the treated tumour cells only after light irradiation (Fig. S27g†), not in dark treatments.

Furthermore, the capacity of the compounds to yield singlet oxygen species is negatively associated with the Nrf2 levels inside the treated and photoirradiated cells (ESI† Fig. S27i), and an inverse association between ROS and Nrf2 was also observed when cells were subjected to photoirradiation (ESI† Fig. S27f). Consequently, the protective effect that Nrf2 can confer to tumour cells subjected to porphyrin treatment will be negated when photoirradiation is applied on the cells previously incubated with a porphyrin derivative.

3. Conclusion

The synthesis of *meso*-substituted AB_3-type porphyrins **2** and **4**, which contain a phenothiaznyl or ferrocenylvinyl-phenothiazinyl moiety in the *meso*-position of the porphyrin unit, has been successfully achieved through the Suzuki–Miyaura or Mizoroki–Heck cross-coupling reactions, respectively. The newly synthesised indium(III) or zinc(II) complexes were obtained in satisfactory yields (34–43%) by the complexation reaction of the free base porphyrins with $InCl_3$ or $Zn(AcO)_2$, respectively.

In both cases, in solution and after internalisation into A2780 cells, the newly synthesised porphyrins show an intense red fluorescence. In comparison with the free base porphyrin precursors (**2** Φ_F = 1%, and **5** Φ_F = 3%), all the In(III) porphyrin complexes (**2a** Φ_F = 30%, **4a** Φ_F = 29%, **5a** Φ_F = 28%) show a higher quantum yield of fluorescence emission in solution. The fluorescence imaging showed that all porphyrins and their metal complexes were able to be internalised into A2780 cells, with the cells exhibiting intense

 This journal is © The Royal Society of Chemistry 2025

Open Access Article. Published on 28 October 2024. Downloaded on 12/5/2025 5:05:15 PM. This article is licensed under a Creative Commons Attribution-NonCommercial 3.0 Unported Licence.

red fluorescence after internalisation. The experimental data indicates that the incorporation of phenothiazine units and indium(III) ion into porphyrin scaffolds does not appreciably enhance the generation of singlet oxygen, when compared to the tetraphenylporphyrin (TPP) **6** and In(III) analogue **6a**. In the series of novel *meso*-substituted phenothiazinyl-porphyrins, the highest singlet oxygen quantum yield was recorded for In(III) ferrocenylvinyl-phenothiazinylporphyrin **4a** ($\Phi_\Delta(^1O_2)$ = 60%).

The most potent cytotoxicity against the A2780 cells, as reflected by IC_{50} values, was observed for In(III) ferrocenylvinyl-phenothiazinyl porphyrin **4a** (36.38 μM), while the In(III) phenothiazinyl porphyrin complexes **2a** (287.84 μM) and **5a** (459.56 μM) are less cytotoxic.

The alteration in mitochondrial function of A2780 cells incubated with porphyrins, studied in the dark and under photoirradiation, demonstrates a decrease of metabolic activity among cells treated with **4a**, **4b**, and **6a** in the absence of light, however, no considerable reduction in metabolic activity was observed under photoirradiation.

The general trend of Nrf2 levels was a decrease when the cells were treated and then photoirradiated. Oxidative stress, tumour necrosis factor-alpha (TNF-α) and Nrf-2 activation were particularly pronounced when A2780 cells were treated with **4a** followed by light irradiation. The observed synergy can be attributed to the presence of the ferrocenyl group in combination with indium in this molecule.

The *in vitro* experiments on A2780 cells demonstrated that biological characteristics with the potential to facilitate tumour growth inhibition could be enhanced by indium-functionalised porphyrins under light irradiation. Specifically, the In(III) porphyrin **4a** bearing a ferrocenyl group has been identified as the most active among its analogues.

4. Material and methods

UV-vis spectra were recorded in dichloromethane using a Perkin Elmer Lambda 35 spectrophotometer, in the range 250–900 nm. Fluorescence spectra were measured in dichloromethane using a Perkin Elmer 55 PL spectrophotometer. Elemental analysis (C, H, N, and S) was obtained on a Thermo Scientific Flash EA 1112 elemental analyser. HRMS were performed on Thermo Scientific LTQ Orbitrap XL mass spectrometer ESI or APCI ionization mode. MALDI-TOF were performed on Bruker Daltonics flexAnalysis. The nuclear magnetic resonance (NMR) spectra were recorded on a Bruker Avance spectrometer (400 and 600 MHz).

4.1 Synthesis

The synthesis of phenothiazinyl-boronic acid esters **1** is presented in ESI,† the bromo-phenothiazinyl-porphyrin **3** was synthesized as reported in ref. 13 and phenothiazinyl-bromophenylporphyrin **5** as reported in ref. 32.

10-Ethyl-7-(4-(10,15,20-triphenylporphyrin-5-yl)phenyl)-10*H*-phenothiazine-3-carbaldehyde (2). The 5-(4-bromophenyl)-10,15,20-triphenylporphyrin (1 g, 1.44 mmol), (10-ethyl-7-formyl-10*H*-phenothiazin-3-yl)boronic acid (0.82 g, 2.88 mmol), anhydrous K_2CO_3 (1.6 g, 11.5 mmol) and 15% $Pd(PPh_3)_4$ (0.25 g, 0.2 mmol) were weighed into a 50 ml Schlenk tube. The flask was pump-purged with nitrogen three times. Nitrogen degassed toluene/DMF (v/v 2/1) was added, freeze/pump/thawed three times under a nitrogen, and the reaction mixture was stirred at 100 °C for 2 d. Toluene (25 mL) and H_2O (25 mL) were added to the reaction mixture. The organic phase was extracted, dried with Mg_2SO_4, and filtered. The filtrate was concentrated and precipitated with hexane. The precipitate was washed with 100 mL hexane to remove the traces of DMF. Column chromatography on silica with dichloromethane afford the title compound as red-purple powder. Yield: 0.26 g, 21%.

Elemental Anal. Calcd. for $C_{59}H_{41}N_5SO$: C, 81.63; H, 4.76; N, 8.07; found: C, 81.74; H, 4.95; N, 7.83;

^{1}H-NMR (400 MHz, $CDCl_3$): δ ppm −2.71 (s, 2H, NH), 1.52 (t, 3H, H_b), 4.02 (q, 2H, H_a), 6.92 (d, 1H, H_9, ^3J = 8.4 Hz), 7.03 (d, 1H, H_1, ^3J = 8.44 Hz), 7.62–7.65 (m, 4H, H_6, H_8, H_2, H_4), 7.73–7.79 (m, 9H, H_c, H_d), 7.88 (d, 2H, $H_{b'}$, ^3J = 8 Hz), 8.22–8.26 (m, 8H, H_b, $H_{c'}$), 8.87–8.93 (m, 6H, H_{pyr}), 8.93 (d, 2H, H_{pyr}, ^3J = 5 Hz), 9.80 (s, 1H, $H_{3'}$);

^{13}C-NMR (100 MHz, $CDCl_3$): δ ppm 12.9 (CH_3, C_b), 42.7 (CH_2, C_a), 114.4, 116.0, 119.7, 120.3, 123.9, 124.1, 124.8, 126.1, 126.5, 126.8, 127.8, 130.4, 131.2, 134.7, 135.2, 136.3, 138.8, 141.3, 142.3, 142.5, 150.0, 190.1 (CH, $C_{3'}$);

MALDI-TOF (in DCTB): Calcd: 867.30, found: 867.29.

HRMS ESI$^+$ Calcd. for $C_{59}H_{41}N_5OS$ [M + H] 868.31046, found [M + H] 868.30902.

5-(4-(10-Ethyl-7-formyl-10*H*-phenothiazin-3-yl)phenyl)-10,15,20-triphenyl-21,23-indium chloride-porphyrin (2a). The porphyrin **2** (0.1 mmol, 0.86 g), $InCl_3$ (0.15 mmol, 0.033 g) and sodium acetate (0.7 mmol, 0.057 g) were added to 25 ml of acetic acid. The mixture was refluxed for 8 hours, after which the resulting solution was cooled to room temperature. The obtained precipitate was washed with distilled water and recrystallised from a solvent system comprising DCM and heptane (v/v 1/1).

Purple powder, yield 43%.

Elemental Anal. Calcd. for $C_{59}H_{39}ClInN_5OS$: C, 69.73; H, 3.87; N, 6.89; S, 3.15; found: C, 69.68, H, 3.92, N, 6.83, S, 3.21.

^{1}H-NMR (400 MHz, $CDCl_3$): δ ppm 1.53 (t, 3H, H_b), 4.06 (q, 2H, H_a), 6.96 (d, 1H, H_9, ^3J = 8.4 Hz), 7.09 (d, 1H, H_1, ^3J = 8.4 Hz), 7.64–7.82 (m, 13H, H_6, H_8, H_2, H_4, H_c, H_d), 7.92 (d, 1H, ^3J = 7.9 Hz), 7.98 (d, 1H, ^3J = 7.9 Hz), 8.14 (d, 3H, ^3J = 7.5 Hz), 8.18 (d, 1H, ^3J = 7.8 Hz), 8.38–8.41 (m, 3H), 8.44 (d, 1H, ^3J = 7.8 Hz), 9.09–9.11 (m, 6H, H_{pyr}), 9.16 (d, 2H, H_{pyr}, ^3J = 4.6 Hz), 9.81 (s, 1H, $H_{3'}$);

^{13}C-NMR (100 MHz, $CDCl_3$): δ ppm 18.4 (CH_3, C_b), 42.7 (CH_2, C_a), 114.4, 115.9, 121.3, 121.8, 123.89, 123.99, 124.8, 126.1, 126.4, 126.8, 126.9, 130.4, 131.0, 134.3, 135.1, 136.0, 139.0, 140.8, 141.7, 142.5, 149.5, 190.1 (CH, $C_{3'}$);

Open Access Article. Published on 28 October 2024. Downloaded on 12/5/2025 5:05:15 PM.
This article is licensed under a Creative Commons Attribution-NonCommercial 3.0 Unported Licence.

HRMS (ESI$^+$) Calcd. for: $C_{59}H_{39}ClInN_5OS$ [M$^+$] 1015.15971, found: 1015.15802.

5-(7-((Ferrocene-1-yl)vinyl)-10-methyl-10*H*-phenothiazin-3-yl)-10,15,20-triphenyl-21,23*H*-porphyrin (4). The 3-bromo-10-methyl-7-(10,15,20-triphenylporphyrin-5-yl)-10*H*-phenothiazine **3** (1 eq., 100 mg, 0.10 mmol), vinyl ferrocene (50-fold excess, 1.3 g, 6.13 mmol), PdOAc (0.15 eq., 5 mg, 0.02 mmol), NaOAc (6 eq., 60 mg, 0.73 mmol) and triphenylphosphine (0.4 eq., 13 mg, 0.049 mmol) were added to a Schlenk tube and purged with argon. Subsequently, dry DMF/toluene (1 : 1) was added to the Schlenk tube, the obtained mixture was heated to 105 °C for 48 hours (TLC control) in an inert atmosphere. The crude product was extracted with chloroform and washed with water. The organic layer was collected and dried with Na_2SO_4, and the solvent was evaporated under reduced pressure. The residue was subjected to column chromatography on silica gel, with the eluent consisting of chloroform/hexane (1 : 1). Purple powder, yield 26% (0.03 g).

Elemental Anal. Calcd. for $C_{61}H_{43}FeN_5S$: C, 78.45; H, 4.64; Fe, 5.98; N, 7.50; S, 3.43; found: C, 78.62; H, 4.72, N, 7.84, S, 3.51.

^{1}H-NMR (400 MHz, $CDCl_3$) δ ppm −2.74 (s, 2H, NH), 3.67 (s, 3H, CH_3), 4.17 (s, 5H, H_{Cp}), 4.31 (s, 2H, H_{Cp}), 4.49 (s, 2H, H_{Cp}), 6.67 (d, 1H, ^3J = 16.0 Hz, $H_{2'}$), 6.83 (d, 1H, ^3J = 16.0 Hz, $H_{1'}$), 6.98 (d, 1H, ^3J = 8.4 Hz, H_9), 7.19 (d, 1H, ^3J = 8.0 Hz, H_1), 7.34 (d, 1H H_8), 7.41 (s, 1H, H_6), 7.77–7.79 (m, 9H, $H_{b,c}$), 8.01 (d, 1H, H_2), 8.06 (s, 1H, H_4), 8.24 (d, 6H, H_a), 8.87 (s, 6H, H_β), 8.93 (d, 2H, ^3J = 4.4 Hz, H_β);

^{13}C-NMR (100 MHz, $CDCl_3$) δ ppm 35.5 (CH_3), 66.5 (2C_{Cp}), 68.7 (2C_{Cp}), 69.0 (5C_{Cp}), 83.3 (C_{Cp}), 111.9 (CH), 114.1 (CH), 119.8 (CH), 120.95 (C), 120.97 (C), 121.0 (C), 123.3 (C), 123.9 (C), 124.4 (C), 125.3 (C), 125.4 (C), 126.3 (6CH), 126.4 (3CH), 127.3 (2CH), 131.7 (6CH), 131.8 (CH), 132.6 (CH), 132.7 (C), 133.5 (C), 134.23 (4CH), 134.26 (CH), 134.28 (4CH), 136.9 (C), 142.6 (4C), 144.2 (C), 144.8 (C), 150.01 (2C), 150.02 (2C) 150.04 (C), 150.1 (C).

HRMS (APCI$^+$) Calcd. for: $C_{63}H_{45}N_5SFe$ [M + H$^+$] 960.28179, found: 960.28027.

5-(7-((Ferrocene-1-yl)vinyl)-10-methyl-10*H*-phenothiazin-3-yl)-10,15,20-triphenyl-21,23-indium(III)chloride-porphyrin (4a). The porphyrin **4** (96 mg, 0.10 mmol), $InCl_3$ (33.15 mg, 0.15 mmol), and sodium acetate (57.4 mg, 0.70 mmol) were added to 25 ml of acetic acid. The mixture was then refluxed for eight hours, after which the resulting solution was cooled to room temperature. The precipitate that had formed was filtered, washed with distilled water, and recrystallised from a solvent system comprising dichloromethane and heptane in a volumetric ratio of 1/1.

Purple powder, yield 43% (47 mg).

Elemental Anal. Calcd. for $C_{44}H_{28}ClN_4In$: C, 69.26; H, 3.70; N, 7.34; found: C, 69.20, H, 3.68, N, 7.23. ^{1}H-NMR (600 MHz, $CDCl_3$) δ ppm 3.62 (s, 3H, CH_3), 4.13 (s, 5H, H_{Cp}), 4.26 (s, 2H, H_{Cp}), 4.44 (s, 2H, H_{Cp}), 6.63 (d, 1H, ^3J = 15.8 Hz, $H_{2'}$), 6.78 (d, 1H, ^3J = 15.8 Hz, $H_{1'}$), 6.93 (d, 1H, ^3J = 8.2 Hz, H_9), 7.02 (d, 1H, H_1), 7.14–7.35 (m, 2H, $H_{6,8}$), 7.74–7.76 (m, 9H, $H_{b,c}$), 7.98–8.00 (m, 2H, $H_{2,4}$), 8.22 (d, 6H, H_a), 8.94 (d, 6H, H_β), 9.01 (d, 2H, ^3J = 4.7 Hz, H_β);

^{13}C-NMR (150 MHz, $CDCl_3$) δ ppm 36.1 (CH_3), 67.1 (2C_{Cp}), 69.4 (2C_{Cp}), 69.66 (5C_{Cp}), 83.9 (C_{Cp}), 112.6 (CH), 114.7 (CH), 120.4 (CH), 121.5 (CH), 12.6 (CH), 121.7 (CH), 124.0 (C), 124.6 (C), 125.1 (C), 125.9 (C), 126.0 (3CH), 126.8 (3CH), 127.0 (CH), 127.9 (CH), 129.2 (CH), 130.1 (CH), 132.3 (CH), 132.43 (6CH), 132.48 (CH), 133.3 (C), 133.4 (C), 134.1 (4CH), 134.87 (4CH), 134.89 (4C), 134.9 (C), 137.5 (C), 143.2 (4C), 144.2 (C), 144.9 (C), 145.4 (C), 150.64 (C), 150.66 (C), 150.68 (C), 150.7 (2C).

HRMS (ESI$^+$) Calcd. for: $C_{63}H_{43}ClFeInN_5S$ [M$^+$] 1107.13104, found: [M–Cl$^+$] 1072.16479.

5-(7-((Ferrocene-1-yl)vinyl)-10-methyl-10*H*-phenothiazin-3-yl)-10,15,20-triphenyl-21,23-Zn(II)-porphyrin (4b). The porphyrin **4** (96 mg, 0.10 mmol) $Zn(OAc)_2$ (56 mg, 0.30 mmol) were added to 20 ml DMF. The mixture was then refluxed for six hours, after which the resulting solution was cooled to room temperature. The reaction mixture was poured into the water and the precipitate that had formed was filtered. The residue was subjected to column chromatography on silica gel, with the eluent consisting of chloroform/hexane (1 : 1). Purple powder, yield 30% (30 mg).

Elemental Anal. Calcd. for $C_{63}H_{43}FeN_5SZn$: C, 73.94; H, 4.24; N, 6.84; S, 3.13 found: C, 73.87; H, 4.27; N, 6.78; S, 3.21.

^{1}H-NMR (400 MHz, $CDCl_3$) δ ppm 3.62 (s, 3H, CH_3), 4.13 (s, 5H, H_{Cp}), 4.27 (s, 2H, H_{Cp}), 4.45 (s, 2H, H_{Cp}), 6.63 (d, 1H, ^3J = 16.0 Hz, $H_{2'}$), 6.81 (d, 1H, ^3J = 16.0 Hz, $H_{1'}$), 6.95 (d, 1H, ^3J = 8.4 Hz, H_9), 7.14 (d, 1H, H_1), 7.28–7.32 (m, 2H, $H_{6,8}$), 7.71–7.78 (m, 9H, $H_{b,c}$), 7.97–7.99 (m, 2H, $H_{2,4}$), 8.21 (d, 6H, H_a), 8.94 (d, 6H, H_β), 9.00 (d, 2H, ^3J = 4.5 Hz, H_β);

^{13}C-NMR (100 MHz, $CDCl_3$) δ ppm 35.8 (CH_3), 66.8 (2C_{Cp}), 69.1 (2C_{Cp}), 69.3 (5C_{Cp}), 83.6 (C_{Cp}), 112.3 (CH), 114.4 (CH), 120.1 (CH), 121.26 (CH), 121.28 (CH), 121.4 (CH), 124.2 (C), 124.7 (C), 125.7 (C), 126.6 (6CH), 126.7 (3CH), 127.6 (CH), 128.9 (CH), 129.8 (CH), 132.0 (CH), 132.12 (6CH), 132.16 (CH), 133.0 (C), 133.09 (C), 133.8 (C), 134.55 (4CH), 134.58 (2CH), 134.6 (2CH), 142.9 (4C), 144.5 (C), 150.32 (2C), 150.34 (4C), 150.4 (2C).

HRMS (APCI$^+$) Calcd. for: $C_{63}H_{43}FeN_5SZn$ [M + H$^+$] 1021.18746, found: 1021.18738.

5-(10-Methyl-10*H*-phenothiazin-3-yl)-10,15,20-tris(4-bromophenyl)-21,23-indium(III)chloride-porphyrin 5a. The porphyrin **5** (0.1 mmol, 98.6 mg), $InCl_3$ (0.15 mmol, 33.15 mg) and sodium acetate (0.7 mmol, 57.4 mg) were added in acetic acid (25 ml). The mixture was refluxed for 8 h, then the resulting solution was cooled down to room temperature, and the precipitate obtained was washed with distilled water and recrystallized from solvent system DCM and heptane (v/v 1 : 1).

Purple powder, yield 34% (34 mg).

Elemental Anal. Calcd. for $C_{51}H_{30}ClInN_5S$: C, 53.98; H, 2.66; N, 6.17; S, 2.82; found: C, 54.03, H, 2.62, N, 6.23, S, 2.78.

^{1}H NMR (400 MHz, $CDCl_3$): δ ppm 3.67 (3H, s, CH_3), 7.07–7.04 (2H, m, H_1, H_9), 7.34–7.23 (3H, m, H_6, H_7, H_8), 7.99–7.90 (10H, m, H_{Ph}), 8.25–8.15 (m, 5H, H_2, H_4, H_{Ph}), 9.06 (6H, d, H_β, ^3J = 4.7 Hz), 9.18 (2H, d, H_β, ^3J = 4.7 Hz), ^{13}C-NMR (100 MHz, $CDCl_3$) δ ppm 32.0 (CH_3), 112.8 (CH), 114.6 (CH), 120.4 (2C), 120.6 (2C), 123.1 (C), 128.0 (6CH), 130.2 (8CH), 130.3

Open Access Article. Published on 28 October 2024. Downloaded on 12/5/2025 5:05:15 PM. This article is licensed under a Creative Commons Attribution-NonCommercial 3.0 Unported Licence.

(CH), 132.81 (CH), 132.87 (CH), 132.9 (CH), 133.4 (CH), 135.6 (6CH), 135.69 (CH), 136.5 (CH), 140.6 (3C), 145.7 (C), 149.2 (C), 149.3 (C), 149.4 (C).

HRMS (ESI$^+$) Calcd. for: $C_{51}H_{30}Br_3N_5SInCl$ [M$^+$] 1132.84734, found [M–Cl$^+$]: 1097.87924.

4.2 Singlet oxygen quantum yield

The DMSO solutions containing the porphyrin derivative and DPBF were irradiated by an LED lamp from Thorlabs (New Jersey, United States) emitting light at a wavelength of 505 nm with a total beam power of 240 mW. The irradiation was conducted in a quartz cuvette (2 mm light path), within a black box, at a temperature of 23 °C, with a distance of 3.5 cm between the light source and the cuvette.

The $^1O_2$ release was monitored by measuring the decrease in the absorbance spectrum of DPBF at 417 nm (ESI† Fig. S5). Absorbance readings were taken every 30 seconds during irradiation, for a total duration of 150 seconds. Thus, the singlet oxygen quantum yields for each compound were calculated according to the following equation:

$$\Phi_\Delta\left(^1O_2\right)^{\text{compound}} = \Phi_\Delta\left(^1O_2\right)^{\text{TPP}} \frac{S^{\text{compound}} \cdot F^{\text{TPP}}}{S^{\text{TPP}} \cdot F^{\text{compound}}}$$

where $\Phi_\Delta(^1O_2)^{\text{compound}}$ is the singlet oxygen quantum yield of porphyrin derivatives **2**, **2a**, **4**, **4a**,**b**, **5**, **5a**, **6a** and $\Phi_\Delta(^1O_2)^{\text{TPP}}$ represents the singlet oxygen quantum yield of TPP ($\Phi_\Delta(^1O_2)^{\text{TPP}}$ = 0.52 in DMSO[33]). S represents the slope of the absorbance difference of DPBF over time (at 417–423 nm) and F is the absorption correction factor, which is given by $F = 1 - 10^{-\text{OD}}$ (OD at the irradiation wavelength). Control measurements were carried out in the same experimental conditions on pure DMSO solution of DPBF and all free solution of porphyrin derivative **2**, **2a**, **4**, **4a**,**b**, **5**, **5a**, **6a** compounds, at a concentration of 10^{-5} M. The solution of the investigated porphyrin was irradiated for a total of 150 seconds in the absence of DPBF in order to evaluate the porphyrin stability during the photodynamic investigations. No degradation of porphyrins was recorded in UV-vis spectra during the 150 second irradiation using an LED source at a wavelength of 505 nm.[36,40]

4.3 Cell cultivation

We performed an *in vitro* testing on A2780 ovarian carcinoma cell line, acquired from the European Collection of Authenticated Cell Cultures (ECACC, Salisbury, Great Britain). The general instrumentation of the cell culture laboratory comprises class II biological safety cabinets (Streamline BSC from Esco Lifesciences Group, Singapore); incubators with controlled CO_2 atmosphere (Galaxy 48RCO_2, provided by Eppendorf AG, Hamburg, Germany); centrifuges with spin-out and cytocentrifugation rotors (Universal 32 and 32R from Hettich Technology, Tuttlingen, Germany); thermostatic platform shaker (Titramax 1000 from Heidolph Instruments GmbH, Schwabach, Germany); inverted phase microscope CX41 and optical microscope BX40 (both from Olympus, Tokyo, Japan); automatic cell counter (EVE from NanoEnTek, Seoul, Korea) and orbital shaker (PSU-10i from BioSan, Riga, Latvia). The cells were cultivated and propagated in RPMI-1640 cell culture media, supplemented with 10% fetal calf serum (FCS), on 25 cm^2 cell culture Nunclon flasks (from Nunc, through Thermo Fisher Scientific, Waltham, MA, USA); the cell passages were completed at about 80–85% confluency by detaching the cell layer with 0.25% Trypsin-EDTA solution and seeding on new flasks (all media, supplements, enzymes from Sigma Aldrich, through Merck KGaA, Darmstadt, Germany). From each passage, a batch of 2 × 10^6 cells were mycoplasma tested (stained with Hoechst 33342 dye) and analyzed by an Eclipse E600 fluorescence microscope from Nikon, and stored in cryoconservation vials (from Nunc, Roskilde, Denmark) at −190 °C in a liquid nitrogen locator (Cryosystem 2000 from MVE, Burnsville, MN, USA). The cells were further seeded on 96-well microplates, 4-well assay plates, or 6-well assay plates (all plates manufactured by Nalgene Nunc, Allerd, Denmark), according to the experiment, as described in the following paragraphs.

4.4 Compounds dissolution for biologic testing

Eight novel synthesized tetraphenylporphyrin compounds were weighted and dissolved in dimethyl sulfoxide (DMSO, from MerckKGaA, Darmstadt, Germany) to obtain 10 mM stock solutions: **2**, **2a**, **4**, **4a**, **4b**, **5**, **5a**, **6**, **6a**.

As reference tetraphenylporphyrin **6** (10 mM stock solution in DMSO) and the standard platinum-based drug: carboplatin (10 mg mL^{-1}, form Teva Pharmaceutical Industries Ltd, Tel Aviv, Israel) were used.

Working solutions were prepared, by mixing the stock solution with RPMI-1640 cell culture media, to obtain 8 successive dilutions between 5 and 0.05 mM for each novel compound from **2** to **6a**, the ref. 6 and carboplatin.

4.5 Cytotoxicity

For cytotoxicity evaluation, a cell suspension of 10^5 cells per mL was prepared in RPMI-1640, dispensed on 96-well assay plates (190 μL in each well) and incubated for 24 hours at 37 °C, then treated with 10 μL of **2** to **6a**, **6** and carboplatin, with a final concentration in culture media of 500; 250; 125; 62.5; 31.25, 15.6; 7.8 and 3.9 μM, in triplicates (n = 9). Following a 24 hours incubation, the solutions were aspirated and replaced with 1% MTT (3,5-dimethylthiazolyl-diphenyl-tetrazolium bromide) solution in Hank's balanced salt solution (both from Sigma Aldrich). After a 1 hour incubation, the MTT solution was removed and 150 μL of DMSO was added to each well to dissolve the formazan salts. Cell viability was assessed by measuring absorbance at 570 nm using a Synergy LX multimode plate reader provided by BioTek Company, Winooski, VT, USA. Baseline-correction of the absorbance values were done by subtracting the blank values (wells handled with media

Open Access Article. Published on 28 October 2024. Downloaded on 12/5/2025 5:05:15 PM.
This article is licensed under a Creative Commons Attribution-NonCommercial 3.0 Unported Licence.

only, without cells). The percentage of viability was calculated related to the untreated control wells, considered as 100% viability. To test the toxicity of the DMSO solvent, used to prepare stock solutions, a series of DMSO-solutions were tested on cells: 2.5; 2; 1.5; 1; 0.5; 0.25; 0.1 and 0.05 and 0.025%, same as the concentrations of DMSO in the cell culture media after we added the serial dilutions of each compound onto the cells. None of these concentrations showed inhibition of cells viability.

4.6 Cellular uptake

The A2780 cells were seeded onto 35 mm imaging dishes with a coverslip bottom (from Ibidi, Graefelfing, Germany), at a concentration of 2×10^5 cells per mL in cell culture media containing 20 μM porphyrin solutions. Following 24 hours and 72 hours incubation, respectively, the media was collected from every dish, the surface was rinsed with PBS buffer at room temperature, and the cells were fixed to the surface by dispensing 4% paraformaldehyde solution, prepared in-house by dissolving paraformaldehyde powder (from Sigma Aldrich) in PBS. After 20 minutes incubation at room temperature, dishes were rinsed with cold PBS, filled with a thin layer of PBS. Fluorescence and bright field images were captured using an Axio Observer Z1 inverted microscope equipped with a Compact Light Source HXP 120 C mercury lamp (Carl Zeiss, Oberkochen, Germany). An AxioCam Mrm digital camera, a 20× and a 63× objectives were used. To visualize the fluorescence of the compounds, the Rhod-set 20 (excitation: BP 546/12, emission: BP 575–640) was employed, while in order to visualize the fluorescence of DAPI, coming from the nucleus, we used set 49 (excitation: G 365, emission: BP 445/50). Data was processed using the ZEN Digital Imaging for Light Microscopy software.

4.7 Photoactivation of the internalized compounds

The A2780 cells were seeded on 4-well Nunclon culture plates, at a concentration of 2×10^5 cells in 1 mL cell culture media containing 20 μM of **2**, **2a**, **4**, **4a**, **4b**, **5**, **5a**, **6**, **6a** or carboplatin, for 24 hours. For every compound, 3 wells were filled with cells subjected to the same treatment, and in the fourth well PBS was dispensed. As reference, a plate was prepared with cells suspended in cell culture media only, without any treatment. These samples were used as unirradiated reference; there were incubated for 24 hours in a humidified incubator.

For irradiation, performed with the same 505 nm LED, power of 240 mW, (irradiation time 150 s), on each 4-well plate only one well was loaded with cells, and in the rest the same volume of PBS was dispensed. The shape and diameter of the assay well on the 4-well microplate is comparable with the photoirradiation's main beam spot size, allowing the exposure of the whole surface. In this procedure the option was to fill with cell suspension one well of the plate to avoid multiple irradiations of the same microplate and to circumvent the accidental exposure of the cells from the well's periphery to the secondary illumination beam while irradiating a well from the vicinity. Therefore 3 independent plates were used for each compound to obtain triplicates. Untreated cells were subjected to irradiation in the same way, to obtain an irradiated, non-treated reference. After the photoirradiation, the plates were placed in the same incubator with the non-irradiated 4-well plates and incubated for 24 hours.

The cell media was collected from all plates and dispensed into 1.8 ml Nunclon cryovials (from Thermo Fisher Scientific, Waltham, MA, USA), centrifuged at 10 000 RPM using an ultracentrifuge (Microfuge 3135 from Abbott GmbH, Ludwigshafen, Germany) and about 1 mL supernates were cryoconserved at −80 °C (ultrafreezer from Heto Holten, Denmark), to obtain triplicate cell culture media samples for each treatment. Meanwhile, the wells were rinsed gently with phosphate buffered salt solution (PBS, from Sigma Aldrich) at room temperature, and the cells were harvested, washed with PBS, counted with the automatic cell counter (from NanoEnTek, Seoul, Korea). Each sample was divided in aliquots, for two tests: the ROS assessment and ELISA quantitative measurement of Nrf-2 and NF-κB. Half of the harvested cells were resuspended in 1 ml cold sterile ultrapure water (from Sigma Aldrich) in polycarbonate centrifuges tubes (from Nunc, Thermo Fisher Scientific). The tubes were kept 20 minutes on ice, then placed for 1 minute into the −80 °C ultra freezer (from Heto Holten, Denmark), sonicated and resuspended by pipetting. These consecutive steps were repeated 3 times, until all the cells were mechanically disrupted. The cell lysis was made without lysis solution, to fulfil the pre-requirements of the Nrf2 test. The tubes were centrifuged at 10 000 RPM (Microfuge 3135 ultracentrifuge) and 0.8 mL lysates from each were cryoconserved at −80 °C (ultrafreezer from Heto Holten, Denmark). The rest of the cells were centrifuged at 1000 RPM, and the cell pellet was further used for CM-2HCFDA test.

4.8 Oxidative stress in treated cells

The reactive oxygen species produced in tumour cells were measured with the general oxidative stress indicator CM-H2DCFDA reagent from Invitrogen Corporation, Carlsbad, CA, USA. The cells were cultivated on 4-well plates, treated in triplicates and exposed to the same 505 nm LED, power of 240 mW, counted and harvested as described in 4.8. Photoactivation of the compounds. As reference, we used untreated cell samples. CM-H2DCFDA dye was dissolved in DMSO and diluted in PBS buffer enriched with Ca and Mg (from Sigma Aldrich) to obtain a 20 μM working solution. The cell pellets from each sample were suspended in 400 μL CM-H2DCFDA reagent, incubated for 30 minutes at 37 °C, washed twice with 1 ml cold Hepes buffer (acquired from Sigma Aldrich) and resuspended in 300 μL Hepes. From each sample, 3 aliquots of 100 μL were loaded on 96-well assay plates for fluorescence, with black walls and transparent bottom (acquired from Corning BV, Amsterdam,

Open Access Article. Published on 28 October 2024. Downloaded on 12/5/2025 5:05:15 PM. This article is licensed under a Creative Commons Attribution-NonCommercial 3.0 Unported Licence.

Netherlands). Blank samples were measured by filling the wells with buffer only. The plates were measured at 488 nm/528 nm in fluorescence with the above-mentioned Synergy 2 multimodal plate reader. The fluorescence intensity values were normalized according to the cells density in the samples, and the results were analysed with the GraphPad Prism5 software.

4.9 Metabolic rate evaluation

The cell metabolic rate and the changes in the metabolic activity were quantified based on their intracellular reducing potential, by the Alamar Blue cell viability reagent kit (from Invitrogen Corporation, Carlsbad, CA, USA). The non-fluorescent, blue coloured resazurin from the kit is able to internalize into the living cells, and due to the mitochondrial reducing activity of the viable cells, it will be transformed into the red, intensively fluorescent resorufin derivate, which can be detected and quantified both with colorimetric or fluorescence methods. For the assay, the A2780 cells were distributed onto 96-well plates; in each well 190 μL of cell suspension was added, containing cells at a concentration of 2×10^5 cells per mL in RPMI cell culture media. For each experiment, 3 individual wells were kept untreated, while the media in the other wells was mixed in a proportion of 1 : 20 with four distinctive concentrations of the compounds **2**, **2a**, **4**, **4a**, **4b**, **5**, **5a**, **6** or **6a**. For each compound 4 concentrations were used, in triplicates: 5; 15, 25 and 50 μM final concentration in the cell culture media. The assay plates were placed in humidified incubator at 37 °C and 5%CO_2 for 24 hours, and then the cell culture media was replaced with 1 mL of fresh RPMI-1640 media containing 10% Alamar Blue dye. The plates were incubated with the viability reagent for 3 hours, then subjected to fluorescence measurements at 540 nm/25 excitation and 620 nm/40 emission, using a Synergy LX multimode plate reader provided by BioTek Company, Winooski, VT, USA. The metabolic rate evaluation was completed following the same procedure for the 48 hours and 72 hours exposure of the cells.

The treatments were completed on three successive cell passages. On the non-irradiated 96-well plates colour controls were placed, in the upper and lower side rows of the plates, consisting in cell culture media with treatment only, without cells. Most of the substances **2** to **6a** were coloured, some of them having a tendency to be absorbed onto the bottom of the wells, therefore it was important to evaluate the potential impact of the compounds own colour or fluorescence on the measurements. No interferences were observed with the fluorescence intensity of the Alamar Blue probes, for none of the compounds, although in colorimetry some overlap was measured. Therefore, in the present experiment only the 620 nm fluorescence intensity and polarization values were considered. The results were analysed using the Prism 5 software (GraphPad, La Jolla, CA, USA).

To analyse the metabolic rate of the treated and photoirradiated (PDT) cells, the 96-well plates were loaded with cell suspension with the same volumes and cell densities, but only the four corners of the plates were filled; in each extremity 4 distinct wells were loaded with cells, suspended in 190 μL media. In this way, on each plate four spots were obtained on a surface covered totally by the irradiation beam. In every group 1 well was kept untreated and 3 wells were treated with 10 μL compounds **2**, **2a**, **4**, **4a**, **4b**, **5**, **5a**, **6** or **6a** at the same concentration with the non-irradiated plates: 5; 15, 25 and 50 μM final concentrations. Within 4 hours after the treatment, the plates were irradiated with the same 505 nm LED, power of 240 mW, (irradiation time 150 s), as described in 4.7 and 4.8. After irradiation the plates were placed in the humidified incubator for 24, 48 or 72 hours, stained with Alamar Blue reagent and the 620 nm fluorescence intensity was measured as described earlier. The metabolic activity of the treated *vs.* treated and photoirradiated cells was compared using the one-way Anova test of the above mentioned Prism 5 software.

4.10 Intracellular nuclear factor erythroid 2-related factor 2 (Nrf-2) and nuclear factor kappa light chain enhancer of activated B cells (NF-κB)

The A2780 cell suspension was plated on 4-well Nunclon assay plates, in 1 ml cell culture media, at a concentration of 5×10^5 cells per ml. The cells were treated with the compounds **2**, **2a**, **4**, **4a**, **4b**, **5**, **5a**, **6**, **6a** at 20 μM final concentration in the cell suspension, four different wells were treated with each compound. After 24 hours the media containing **2**, **2a**, **4**, **4a**, **4b**, **5**, **5a**, **6**, **6a**, treatment was removed and changed with fresh media. From each sample, three plates were subjected to irradiation, as described in chapter 4.8, while three samples were kept in incubator, without being irradiated. After another 24 hours, the supernates were removed, and the cells were collected from each well by trypsinization. The supernates were centrifuged at 10 000 RPM, aliquoted and cryoconserved at −80 °C in an ultrafreezer.

The cells collected by trypsinization were washed two times in pre-cooled PBS, resuspended in 500 μL and subjected to repeated sonication, freezing at −80 °C degrees and thawing. After 5 cycles of freezing and sonication, the cells were fully lysed, the lysate was centrifuged at 1500 g for 10 minutes at 4 °C degrees, and the supernatants were collected and freezed at −80 °C degrees. The immune-enzymatic ELISA test was performed for the quantitative evaluation of Nrf-2 in cell culture lysates, with an assay kit for research use, provided by Mybiosource Inc., San Diego, CA, USA. Having a sensitivity of 0.19 ng mL^{-1} and a detection range of 0.31 to 20 ng mL^{-1}, the test detects activated Nrf2 without cross-reactivity with analogues. For the sandwich-ELISA method, the samples were brought at room temperatures, and 8 different serial dilutions were prepared from the recombinant Nrf2 protein standard.

The microplate pre-coated with anti-Nrf2 antibody, provided by the manufacturer, was loaded by pipetting 100

Open Access Article. Published on 28 October 2024. Downloaded on 12/5/2025 5:05:15 PM.
This article is licensed under a Creative Commons Attribution-NonCommercial 3.0 Unported Licence.

μL of standards or samples on each well, in duplicates. The plate was covered with a sealer membrane and incubated at 37 °C degrees for 90 minutes, to allow the combination of the Nrf2 from the samples to the capture antibody. The content of the microwells was discarded, but not washed. 100 μL biotinylated detection anti-Nrf2 antibody was added immediately to each well, and the covered plate was incubated for 1 hour at 37 °C degrees. The microplate was washed 3 times with the solution provided by the manufacturer, using an automated washer (Diasource, Louvain-la-Neuve, Belgium), then the plate was loaded with 100 μL horseradish peroxidase (HRP) conjugate solution and incubated 30 minutes at 37 °C degrees. After another wash cycle, 90 μL substrate reagent was added to each well, and in about 15 minutes the development of coloration was observed, due to the conjugation of the biotinylated detection antibody and avidin-HRP, which provide a blue coloration in the wells where Nrf2 was present. 50 μL acid stop solution was pipetted to each well to stop the enzyme–substrate reaction, and the plate was subjected to optical density measurement at 450/540 nm, using a Sunrise ELISA reader, from Tecan Group (Männedorf, Switzerland) with Magellan software for the data analysis. Based on the standard curve, the software provided quantitative data (concentration of Nrf2 in the cell lysate), in duplicates, for each well.

The transcription factor NF-κB p65 subunit was measured with a semiquantitative ELISA method, from the lysate samples obtained as described in chapter 4.7 using an assay kit (NF-kβ p65 SimpleStep ELISA kit from Abcam, Cambridge, UK), according to the manufacturer's protocol. On the antibody-coated pretreated 96-well plate 50 μL of each sample was added in duplicates. In each well 50 μL of a capture and detection antibody cocktail was added and the plate was incubated 1 hour at room temperature while shaking. Three automatic washing steps were performed using 350 μL wash buffer provided by the kit and 100 μL of TMB substrate was added to each well. After a 15 minutes incubation, 100 μL of stop solution was added to the wells that contains samples or standard solutions and the measurement was performed at 450 nm on TECAN Sunrise ELISA plate reader with Magellan software (Tecan Group, Männedorf, Switzerland). As reference untreated cells were used and the cell culture media without cells was the blank value. A standard curve was obtained using the NF-kβ p65 reference protein provided by manufacturer, and the relative concentration values were calculated.

4.11 Extracellular tumour necrosis factor-alpha (TNF-α)

The extracellular TNF-α level was measured through ELISA testing (kit acquired from Hycult Biotech, Uden, The Netherlands), from the cell culture media. The samples, harvested as described in chapter 4.7 were brought to the room temperature, together with the components of the assay kit. Aliquots of 100 μL of each sample were dispensed to antibody-coated 96-well ELISA plate in duplicates. The lyophilized standard human TNF-α protein was provided by the manufacturer, diluted to obtain 7 serial concentrations, and 100 μL from each solution was dispensed on the testing plate. After 1 hour incubation at room temperature, the plate was washed four times (automated microplate washer from DiaSource Immunoassays, Louvain-La-Neuve, Belgium), 100 μL tracer antibody was added to the wells. The assay plate was incubated for 1 hour, washed and 100 μL of streptavidin–peroxidase solution was dispensed into wells. After another wash cycle, 100 μL of TMB substrate was added to the samples and there were incubated for 30 minutes at room temperature. The assay plate was read at 450/540 nm (Sunrise microplate reader from Tecan Group, Männedorf, Switzerland). The individual TNF-α concentrations of for each sample were established relative to the biologic standards provided by the manufacturer results were analysed with the biostatistics software, triplicate replicate $n = 6$.

Data availability

The data supporting this article have been included as part of the ESI.†

Author contributions

Balázs Brém: investigation, methodology; Bianca Stoean: investigation, formal analysis; Éva Molnár: investigation, formal analysis; Eva Fischer-Fodor: writing – original draft, formal analysis; Ovidiu Bălăcescu: formal analysis; Raluca Borlan: investigation; Monica Focsan: formal analysis; Adriana Grozav: formal analysis; Patriciu Achimaș-Cadariu: formal analysis; Emese Gál: data curation, validation, formal analysis; Luiza Gaina: writing – review & editing, conceptualization, methodology.

Conflicts of interest

There are no conflicts to declare.

Acknowledgements

This work was supported by the project "Targeted Tumor Therapy with multifunctional platinum(IV)-drug conjugates (T^3-Pt)" funded by European Union – NextGenerationEU and Romanian Government, under National Recovery and Resilience Plan for Romania, contract no 760240/28.12.2023, cod PNRR-C9-I8-CF 76/31.07.2023, through the Romanian Ministry of Research, Innovation and Digitalization, within Component 9, "Investment I8". The biologic testing was supported by a grant of the Romanian National Authority for Scientific Research and Innovation (UEFISCDI) project number PN-III-P4-ID-PCE-2021-1572, Metallomex. Luiza Gaina would like to express her gratitude to the "Agence Universitaire de la Francophonie" project AUF DRECO-7867_SER-ECO for its support.

Open Access Article. Published on 28 October 2024. Downloaded on 12/5/2025 5:05:15 PM.
This article is licensed under a Creative Commons Attribution-NonCommercial 3.0 Unported Licence.

References

1 Y. Matoba, K. Banno, I. Kisu and D. Aoki, Photodiagnosis and Photodynamic Therapy Clinical application of photodynamic diagnosis and photodynamic therapy for gynecologic malignant diseases: A review, *Photodiagn. Photodyn. Ther.*, 2018, **24**, 52–57, DOI: **10.1016/j.pdpdt.2018.08.014**.

2 B. Pucelik, A. Sułek, A. Drozd, G. Stochel, M. M. Pereira, S. M. A. Pinto, L. G. Arnaut and J. M. Dabrowski, Enhanced Cellular Uptake and Photodynamic Effect with Amphiphilic Fluorinated Porphyrins: The Role of Sulfoester Groups and the Nature of Reactive Oxygen Species, *Int. J. Mol. Sci.*, 2020, **21**, 2786, DOI: **10.3390/ijms21082786**.

3 H. Kobayashi, S. Imanaka and H. Shigetomi, Revisiting therapeutic strategies for ovarian cancer by focusing on redox homeostasis, *Oncol. Lett.*, 2022, **23**, 80, DOI: **10.3892/ol.2022.13200**.

4 C. Queir, A. Leite, N. M. M. Moura, A. F. R. Cerqueira, V. V. Serra, M. G. P. M. S. Neves, A. C. Tome and A. M. G. Silva, Exploring the reactivity of formylporphyrins with 3-(diethylamino)phenol. Synthesis, spectroscopic properties and singlet oxygen generation of a new porphyrin-rosamine conjugate, *Dyes Pigm.*, 2023, **217**, 111431, DOI: **10.1016/j.dyepig.2023.111431**.

5 D. Li, X. Hong, F. Zhao, X. Ci and S. Zhang, Targeting Nrf2 may reverse the drug resistance in ovarian cancer, *Cancer Cell Int.*, 2021, **21**, 116, DOI: **10.1186/s12935-021-01822-1**.

6 G. Tossetta, S. Fantone, E. Montanari, D. Marzioni and G. Goteri, Role of NRF2 in Ovarian Cancer, *Antioxidants*, 2022, **11**, 663, DOI: **10.3390/antiox11040663**.

7 G. Battogtokh, Y. Su, D. Seop, J. Park, M. Suk, K. Moo, Y. Cho, Y. Lee, H. Suk and H. Chang, Mitochondria-targeting drug conjugates for cytotoxic, anti-oxidizing and sensing purposes: current strategies and future perspectives, *Acta Pharm. Sin. B*, 2018, **8**, 862–880, DOI: **10.1016/j.apsb.2018.05.006**.

8 A. Sułek, B. Pucelik, M. Kobielusz, A. Barzowska and J. M. Dabrowski, Photodynamic Inactivation of Bacteria with Porphyrin Derivatives: Effect of Charge, Lipophilicity, ROS Generation, and Cellular Uptake on Their Biological Activity In Vitro, *Int. J. Mol. Sci.*, 2020, **21**, 8716, DOI: **10.3390/ijms21228716**.

9 F. Schmitt, P. Govindaswamy, O. Zava, G. Suss-Fink, L. Juillerat-Jeanneret and B. Therrien, Combined arene ruthenium porphyrins as chemotherapeutics and photosensitizers for cancer therapy, *J. Biol. Inorg. Chem.*, 2009, **14**, 101–109, DOI: **10.1007/s00775-008-0427-y**.

10 L. Zheng, Z. Li, R. Wang, J. Wang, B. Liu, Y. Wang, S. Qin, J. Yang and J. Liu, Photodiagnosis and Photodynamic Therapy A novel photosensitizer DTPP-mediated photodynamic therapy induces oxidative stress and apoptosis through mitochondrial pathways in LA795 cells, *Photodiagn. Photodyn. Ther.*, 2024, **45**, 103894, DOI: **10.1016/j.pdpdt.2023.103894**.

11 R. Lippert, T. E. Shubina, S. Vojnovic, A. Pavic, J. Veselinovic, J. Nikodinovic-runic, N. Stankovic and I. Ivanovic-Burmazovic, Redox behavior and biological properties of ferrocene bearing porphyrins, *J. Inorg. Biochem.*, 2017, **171**, 76–89, DOI: **10.1016/j.jinorgbio.2017.03.002**.

12 A. R. da Silva, N. Mayumi, D. Rettori, M. Ozello, A. Eugenio and R. A. Jorge, In vitro photodynamic activity of chloro(5,10,15,20-tetraphenylporphyrinato)indium(III) loaded-poly(lactide-co-glycolide) nanoparticles in LNCaP prostate tumour cells, *J. Photochem. Photobiol., B*, 2009, **94**, 101–112, DOI: **10.1016/j.jphotobiol.2008.10.010**.

13 E. Molnar, E. Gal, L. Gaina, C. Cristea, E. Fischer-Fodor, M. Perde-Schrepler, P. Achimas-Cadariu, M. Focsan and L. Silaghi-Dumitrescu, Novel phenothiazine-bridged porphyrin-(Hetero) aryl dyads: Synthesis, optical properties, in vitro cytotoxicity and staining of human ovarian tumor cell lines, *Int. J. Mol. Sci.*, 2020, **21**(9), 3178, DOI: **10.3390/ijms21093178**.

14 H. Horiuchi, M. Hosaka, H. Mashio, M. Terata, S. S. Ishida, T. Kyushin and T. T. Okutsu, Silylation Improves the Photodynamic Activity of Tetraphenylporphyrin Derivatives In Vitro and In Vivo, *Chem. – Eur. J.*, 2014, **20**, 6054–6060, DOI: **10.1002/chem.201303120**.

15 S. Boumati, J. Seguin, G. Beitz, Y. Kaga, M. Jakubaszek, J. Karges, G. Gasser, N. Mignet and B. Doan, Three in One: In Vitro and In Vivo Evaluation of Anticancer Activity of a Theranostic Agent that Combines Magnetic Resonance Imaging, Optical Bioimaging, and Photodynamic Therapy Capabilities, *ACS Appl. Bio Mater.*, 2023, **6**, 4791–4804, DOI: **10.1021/acsabm.3c00565**.

16 Z. Kejik, T. Briza, J. Kralova, P. Pouc, A. Kral, P. Martasek and V. Kral, Coordination conjugates of therapeutic proteins with drug carriers: A new approach for versatile advanced drug delivery, *Bioorg. Med. Chem. Lett.*, 2011, **21**, 5514–5520, DOI: **10.1016/j.bmcl.2011.06.101**.

17 Z. Lei, X. Zhang, X. Zheng, S. Liu and Z. Xie, Porphyrin–ferrocene conjugates for photodynamic and chemodynamic therapy, *Org. Biomol. Chem.*, 2018, **16**, 8613–8619, DOI: **10.1039/c8ob02391c**.

18 H. Ling, J. Bhaumik, J. R. Diers, P. Mroz, M. R. Hamblin, D. F. Bocian, J. S. Lindsey and D. Holten, Journal of Photochemistry and Photobiology A: Chemistry Photophysical characterization of imidazolium-substituted Pd(II), In(III), and Zn(II) porphyrins as photosensitizers for photodynamic therapy, *J. Photochem. Photobiol., A*, 2008, **200**, 346–355, DOI: **10.1016/j.jphotochem.2008.08.006**.

19 N. J. Patel, Y. Chen, P. Joshi, P. Pera, H. Baumann, J. R. Missert, K. Ohkubo, S. Fukuzumi, R. R. Nani, M. J. Schnermann, P. Chen, J. Zhu, K. M. Kadish and R. K. Pandey, Effect of Metalation on Porphyrin-Based Bifunctional Agents in Tumor Imaging and Photodynamic Therapy, *Bioconjugate Chem.*, 2016, **27**, 667–680, DOI: **10.1021/acs.bioconjchem.5b00656**.

20 L. Yang, Y. Liu, X. Ren, R. Jia, L. Si, J. Bao, Y. Shi, J. Sun, Y. Zhong, P. Duan, X. Yang, R. Zhu, Y. Jia and F. Bai, Microemulsion-Assisted Self-Assembly of Indium Porphyrin Photosensitizers with Enhanced Photodynamic Therapy, *ACS Nano*, 2024, **18**, 3161–3172, DOI: **10.1021/acsnano.3c09399**.

21 L. C. Makola, M. Managa and T. Nyokong, Photodiagnosis and Photodynamic Therapy Enhancement of photodynamic

Open Access Article. Published on 28 October 2024. Downloaded on 12/5/2025 5:05:15 PM.
This article is licensed under a Creative Commons Attribution-NonCommercial 3.0 Unported Licence.

antimicrobialtherapy through the use of cationic indium porphyrin conjugated to Ag/$CuFe_2O_4$ nanoparticles, *Photodiagn. Photodyn. Ther.*, 2020, **30**, 101736, DOI: 10.1016/j.pdpdt.2020.101736.

22 R. C. Soy, B. Babu, D. O. Oluwole, N. Nwaji, J. Oyim, E. Amuhaya, E. Prinslooc, J. Mack and T. Nyokong, Photophysicochemical properties and photodynamic therapy activity of chloroindium(III) tetraarylporphyrins and their gold nanoparticle conjugates, *J. Porphyrins Phthalocyanines*, 2019, **23**, 1–12, DOI: 10.1142/S1088424618501146.

23 M. Ojha, M. Banerjee, S. Ray, A. K. Singh, A. Anoop and N. D. P. Singh, Switching photorelease to singlet oxygen generation by oxygen functionalization of phenothiazine photocages, *Chem. Commun.*, 2022, **58**, 2754–2757, DOI: 10.1039/d1cc06950k.

24 E. Baciocchi, T. Del Giacco, O. Lanzalunga, A. Lapi, D. Chimica and I. Cnr, The Singlet Oxygen Oxidation of Chlorpromazine and Some Phenothiazine Derivatives. Products and Reaction Mechanisms, *J. Org. Chem.*, 2007, **72**, 5912–5915, DOI: 10.1021/jo0706980.

25 G. Sivieri-Araujo, H. B. Strazzi-Sahyon, D. P. Jacomassi, P. H. dos Santos, L. T. A. Cintra, C. Kurachi and V. S. Bagnato, Effects of methylene blue and curcumin photosensitizers on the color stability of endodontically treated intraradicular dentin, *Photodiagn. Photodyn. Ther.*, 2022, **37**, 102650, DOI: 10.1016/j.pdpdt.2021.102650.

26 G. B. Rodrigues, G. T. P. Brancini, S. A. Uyemura, L. Bachmann, M. Wainwright and G. U. L. Braga, Chemical features of the photosensitizers new methylene blue N and S137 influence their subcellular localization and photoinactivation efficiency in Candida albicans, *J. Photochem. Photobiol., B*, 2020, **209**, 111942, DOI: 10.1016/j.jphotobiol.2020.111942.

27 M. S. Hameed, Z. M. Alkahtani, M. Ajmal, M. A. Kamran, M. L. Mannakandath and I. Alshahrani, Bond assessment of enamel conditioned with Er, Cr: YSGG laser and methylene blue photosensitizer activated by photodynamic therapy to orthodontic metallic brackets: Enamel Conditioning using Photodynamic therapy and Er, Cr: YSGG, *Photodiagn. Photodyn. Ther.*, 2021, **36**, 102513, DOI: 10.1016/j.pdpdt.2021.102513.

28 B. Stoean, I. Lupan, C. Cristea, M. Silion, L. Silaghi-Dumitrescu, R. Silaghi-Dumitrescu and L. Gaina, Outcomes of folic acid esterification upon the properties of hydrophilic phenothiazinium dyes: New photosensitizers for antimicrobial photodynamic therapy, *J. Photochem. Photobiol., A*, 2024, **451**, 115500, DOI: 10.1016/j.jphotochem.2024.115500.

29 A. Nejadebrahim, M. Ebrahimi, X. Allonas and C. Croutxé-Barghorn, Methylene blue-clay nano-pigment as a new photosensitizer for preparing three-component photoinitiating systems with high thermal stability, *Dyes Pigm.*, 2020, **180**, 108475, DOI: 10.1016/j.dyepig.2020.108475.

30 B. Stoean, D. Rugina, M. Focsan, A. M. Craciun, M. Nistor, T. Lovasz, A. Turza, I. D. Porumb, E. Gál, C. Cristea, L. Silaghi-dumitrescu, S. Astilean and L. I. Gaina, Novel (Phenothiazinyl)vinyl-pyridinium dyes and their potential applications as cellular staining agents, *Int. J. Mol. Sci.*, 2021, **22**, 1–21, DOI: 10.3390/ijms22062985.

31 B. Stoean, L. Gaina, C. Cristea, R. Silaghi-Dumitrescu, A. M. V. Branzanic, M. Focsan, E. Fischer-Fodor, B. Tigu, C. Moldovan, A. D. Cecan, P. Achimas-Cadariu, S. Astilean and L. Silaghi-Dumitrescu, New methylene blue analogues with N-piperidinyl-carbinol units: Synthesis, optical properties and in vitro internalization in human ovarian cancer cells, *Dyes Pigm.*, 2022, **205**, 110460, DOI: 10.1016/j.dyepig.2022.110460.

32 E. Gal, B. Brem, I. Pereteanu, L. Gaina, T. Lovasz, M. Perde-Schrepler, L. Silaghi-Dumitrescu, C. Cristea and L. Silaghi-Dumitrescu, Novel meso-phenothiazinylporphyrin dyes: Synthesis, optical, electrochemical properties and PDT assay, *Dyes Pigm.*, 2013, **99**, 144–153, DOI: 10.1016/j.dyepig.2013.04.034.

33 M. Korínek, R. Dědic, A. Molnár, A. Svoboda and J. Hála, A comparison of photosensitizing properties of meso-tetraphenylporphin in acetone and in dimethyl sulfoxide, *J. Mol. Struct.*, 2005, **744–747**, 727–731, DOI: 10.1016/j.molstruc.2004.11.036.

34 B. Babu, J. Mack and T. Nyokong, Sn(IV) N-confused porphyrins as photosensitizer dyes for photodynamic therapy in the near IR region, *Dalton Trans.*, 2020, **49**, 15180–15183, DOI: 10.1039/d0dt03296d.

35 Y. Liu, L. Luo, H. Zhu, P. Wang, X. Geng and X. Wang, En route to the transformation of porphyrin molecules for PDT: Theoretical insights on the reactive oxygen generation of 1D nano-wires and 2D covalent organic frameworks, *Chem. Phys.*, 2021, **549**, 111278, DOI: 10.1016/j.chemphys.2021.111278.

36 L. Bao, J. Wu, M. Dodson, R. De, V. Yan, N. Zhenbo, M. Yao, D. D. Zhang, C. Xu and X. Yi, ABCF2, an Nrf2 target gene, contributes to cisplatin resistance in ovarian cancer cells, *Mol. Carcinog.*, 2017, **56**, 1543–1553, DOI: 10.1002/mc.22615.

37 J. Wu, L. Bao, Z. Zhang and X. Yi, Nrf2 induces cisplatin resistance via suppressing the iron export related gene SLC40A1 in ovarian cancer cells, *Oncotarget*, 2017, **8**, 93502–93515, DOI: 10.18632/oncotarget.19548.

38 K. Anwer, F. J. Kelly, C. Chu, J. G. Fewell, D. Lewis and R. D. Alvarez, Gynecologic Oncology Phase I trial of a formulated IL-12 plasmid in combination with carboplatin and docetaxel chemotherapy in the treatment of platinum-sensitive recurrent ovarian cancer, *Gynecol. Oncol.*, 2013, **131**, 169–173, DOI: 10.1016/j.ygyno.2013.07.081.

39 D. W. Edwardson, J. Boudreau, J. Mapletoft, C. Lanner, A. T. Kovala and A. M. Parissenti, Inflammatory cytokine production in tumor cells upon chemotherapy drug exposure or upon selection for drug resistance, *PLoS One*, 2017, **12**, e0183662, DOI: 10.1371/journal.pone.0183662.

40 Y. Ooyama, T. Enoki, J. Ohshita, T. Kamimura, S. Ozako, T. Koide and F. Tani, Singlet oxygen generation properties of an inclusion complex of cyclic free-base porphyrin dimer and fullerene C60, *RSC Adv.*, 2017, **7**, 18690–18695, DOI: 10.1039/c7ra02699d.